A THEORETICAL ANALYSIS OF THE CURRENT-VOLTAGE CHARACTERISTICS OF SOLAR CELLS

(NASA-CR-148827) A THEORETICAL ANALYSIS OF THE CURRENT-VOLTAGE CHARACTERISTICS OF SOLAR CELLS Annual Report (North Carolina State Univ.) 98 p HC $5.00 CSCL 10A

N76-32648

Unclas
G3/44 03473

Annual Report on
NASA Grant NGR 34-002-195
NASA Lewis Research Center

August 1976

P. M. Dunbar and J. R. Hauser

Semiconductor Device Laboratory
Department of Electrical Engineering
North Carolina State University
Raleigh, North Carolina 27607

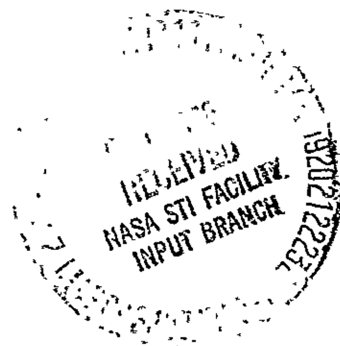

A THEORETICAL ANALYSIS OF THE CURRENT-VOLTAGE CHARACTERISTICS OF SOLAR CELLS

Annual Report on
NASA Grant NGR-34-002-195
NASA Lewis Research Center

August 1976

P. M. Dunbar and J. R. Hauser

Semiconductor Device Laboratory
Department of Electrical Engineering
North Carolina State University
Raleigh, North Carolina 27607

ABSTRACT

This report summarizes work performed during the past twelve months under NASA Grant NGR 34-002-195, entitled A Theoretical Analysis of the Current-Voltage Characteristics of Solar Cells. The overall objective of the work is to identify the various mechanisms which limit the conversion efficiency of silicon solar cells. This is being accomplished by means of a computerized semiconductor device analysis program which gives a complete numerical solution of the general semiconductor device equations including excess carrier generation due to the full spectrum solar irradiance.

The first major area of study concerns the effects of changes in solar cell geometry such as layer thickness on performance. In general it has been found that BSF cells can be reduced in total thickness to the range of 50 μM - 100 μM without a severe loss in conversion efficiency. In fact a slightly improved efficiency was found for cell thicknesses around 100 μM - 150 μM if back surface reflection of light occurs.

The effects of various antireflecting layers have been studied. It is found that any single film antireflecting layer still results in a significant surface loss of photons. The use of surface texturing techniques or low loss antireflecting layers can enhance by several percentage points the conversion efficiency of silicon cells.

The basic differences between n^+-p-p^+ and p^+-n-n^+ cells have been studied. In general the conversion efficiencies of these two types of cells are found to be somewhat equal. The n^+-p-p^+ cell has a slightly

higher conversion efficiency for equal doping levels if the diffusion length for holes is one-half or less of the diffusion length for electrons. If electrons and holes had equal diffusion lengths, the p^+-n-n^+ cell would have a slightly higher conversion efficiency.

A significant part of the study has been devoted to the importance of surface region lifetime and heavy doping effects on efficiency. These effects have been found to be somewhat interrelated with the importance of heavy doping bandgap reduction effects being enhanced by low surface layer lifetimes. Conversely, the reduction in solar cell efficiency due to low surface layer lifetime is further enhanced by heavy doping effects.

Finally a series of computer studies are reported which seek to determine the best cell structure and doping levels for maximum efficiency. Beginning with a fairly standard 10 Ω·cm cell with an efficiency of slightly less than 15%, various modifications are discussed which improve the efficiency to approximately 20%. The most important of these changes are an improved p-p^+ BSF structure, an optimized base layer doping, and a low loss antireflecting layer.

TABLE OF CONTENTS

		Page
1.	INTRODUCTION	1
	1.1 Objectives of Current Work	1
	1.2 Review of Prior Work	3
2.	GEOMETRIC VARIATIONS	12
	2.1 Objectives	12
	2.2 Base Region Width	15
	2.3 Surface Region Widths	20
	2.4 Other Surface Profiles	27
3.	ANTIREFLECTION FILMS	29
	3.1 Back Surface Reflection	29
	3.2 Non-Reflective Antireflection Coatings	30
	3.3 Other Antireflection Films	30
4.	THE P^+-N-N^+ STRUCTURE	36
	4.1 Primary Differences in p^+-n-n^+ and n^+-p-p^+ Structures	36
	4.2 Efficiency as a Function of Base Region Resistivity	37
	4.3 Efficiency as a Function of Base Region Width	41
	4.4 Lifetime Related Differences Between the n^+-p-p^+ and p^+-n-n^+ Structures	44
5.	THEORETICAL EFFECTS OF SURFACE DIFFUSED REGION LIFETIME MODELS ON SILICON SOLAR CELLS	47
	5.1 Introduction	47
	5.2 General Device Models	48
	5.3 Results	52
	5.4 Summary	60
6.	SPECIAL DEVICE STUDIES	63
	6.1 Epitaxial Structures	63
	6.2 "Upside Down" Structure	78
	6.3 Summary	82
7.	SUMMARY	85
8.	LIST OF REFERENCES	92

1. INTRODUCTION

1.1 Objectives of Current Work

The overall objective of the current work is to continue the identification and characterization of various mechanisms which tend to limit the conversion efficiency of silicon solar cells. This includes the study of various geometric variations on the basic three layered structure as well as more complex modifications which involve tailored doping profiles and four layered structures.

As in past work, the results presented in this report represent the results of a complete computer simulation of the solar cell. The attempt is made to formulate a complete theorectical description of a solar cell through a solution of the fundamental device equations, including an external generation rate calculated from tabular information regarding the incident light spectrum, reflection, and the optical properties of the solar cell material. Included within the solution are such phenomena as drift and diffusion current components, doping and field dependent mobility, non-uniform doping profiles, and band gap reduction models due to heavy doping effects. Subsequently the accuracy and completeness of the solutions presented in this report are limited only by the accuracy of contemporary empirical measurement and the realization and understanding of the various subsidiary modeling of second order effects. A detailed discussion of the device modeling and computer analysis program have been presented elsewhere [Dunbar and Hauser (1975)].

Recent developments in solar cell devices have, through textured surfaces and reflecting high-low junctions, increased the short circuit current to closely approach values predicted theoretically. However,

the open circuit voltages obtained experimentally still fall below the various theoretical predictions of what is possible. An investigation of various phenomena which could be the source of these discrepancies forms a major portion of this report.

In addition, many geometric variations of the solar cell structure are investigated. These include rather straightforward studies of region width modification in the basic three layered structure and several of the various two, three and four layered structures which have been recently proposed. A special emphasis is placed upon the major differences between the n^+-p-p^+ and p^+-n-n^+ polarity solar cells due to postulated differences in band gap reduction and lifetime magnitudes. Also studies are shown for various antireflection layers, with a particular enphasis upon "non-reflective" coatings.

1.2 Review of Prior Work

Prior grant periods have been concerned with an extensive analysis and computer simulation of silicon solar cells. The objective of this section is to review and summarize the results of that work and the work of others which have occurred in the same time frame and point out those results which have strong relevance to the present study. For the most part this work was concerned with the operation of both n^+-p and n^+-p-p^+ solar cells of varying base resistivity. The general objective was to identify those physical mechanisms which limit the conversion efficiency.

Figure 1.1 displays the efficiencies of silicon cells as a function of base resistivity. The structural features of the cells are tabulated in Table 1.1. It is to be noted from the table that these are all 250 μM thick solar cells with an 800 Å SiO antireflection layer. For the n^+-p-p^+ structure, the back surface p^+ region is 5 μM in width and doped to $10^{19}/cm^3$. As seen in the figure the efficiency peaks at about 0.3 ohm-cm for the n^+-p-p^+ solar cell and at a slightly lower resistivity for the n^+-p cell. Generally the n^+-p-p^+ solar cell resulted in higher efficiencies than the n^+-p solar cell and gave increases in both the open circuit voltage and the short circuit current.

However, at very low base resistivities no difference was found between the n^+-p and n^+-p-p^+ structures due to the reduction of the p region diffusion length to a value below the p region width. At these low base resistivities injection of holes into the n^+ surface region is also a significant fraction of the total forward dark current. This effect counteracts any increase in open circuit voltage expected from a reduction of center region p type base resistivity. This hole component

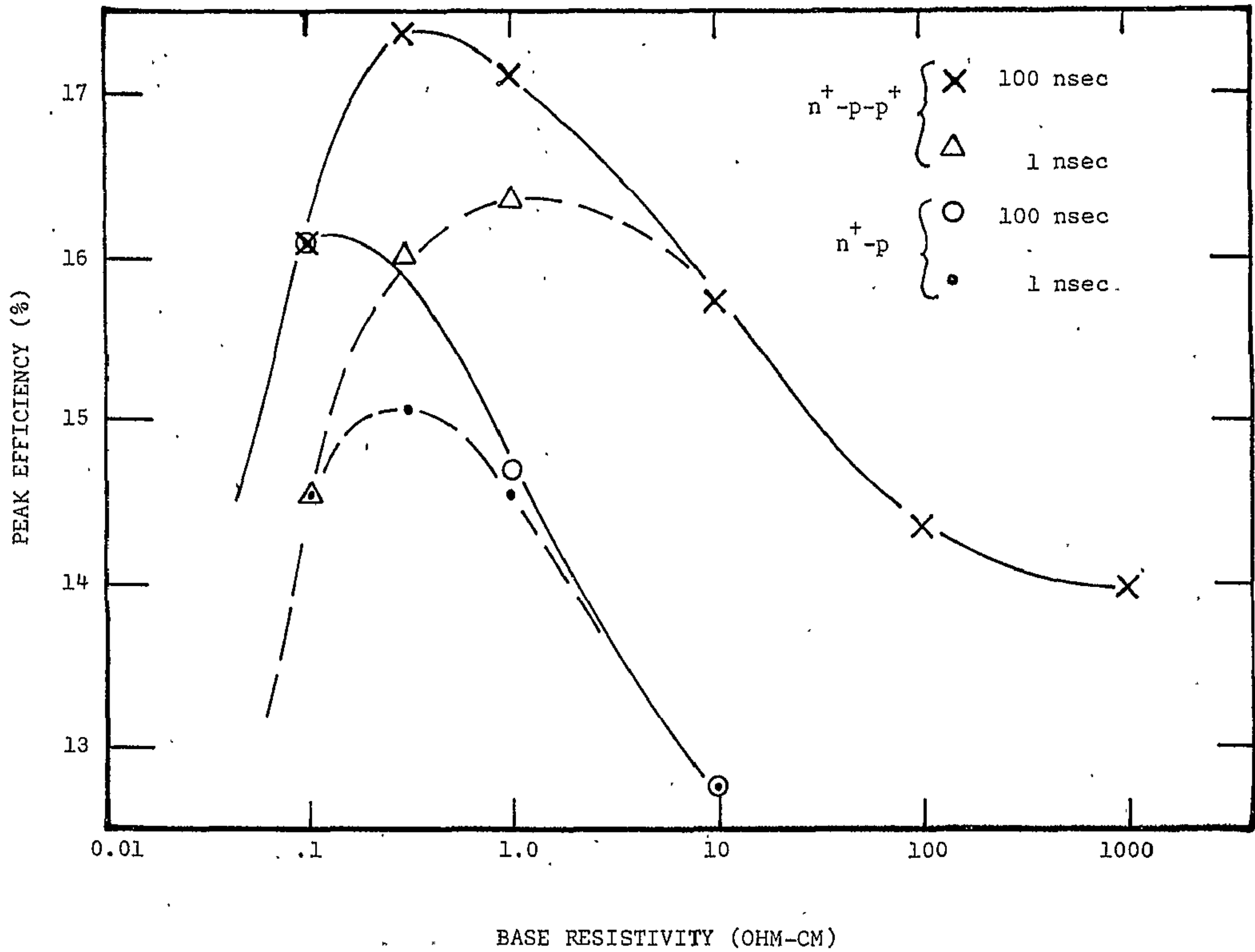

Figure 1.1 Solar cell efficiency as a function of base resistivity (See Table 1.1).

Table 1.1 Material and Dimensional Parameters of Solar Cells Analyzed in Past Work.

Overall Cell Thickness	250 μM
n^+ Thickness	0.25 μM
p^+ Thickness (n^+-p-p^+ cell)	5.0 μM
n^+ Surface Concentration	$10^{20}/cm^3$
p Doping Concentration	Variable
p^+ Doping Concentration	$10^{19}/cm^3$
Lifetime in n^+ Region	100 nsec, 1 nsec
Lifetime in p Region	Iles (1975)
Lifetime in p^+ Region	Iles (1975)
Surface Recombination Velocity	10^3 cm/sec
Antireflection Layer	800 Å, SiO

of forward dark current (so called back injection component) is dependent upon the characterization of the n^+ surface region with respect to heavy doping effects and lifetime. Figure 1.1 for example indicates the large reduction in efficiency for a surface region that has a lifetime of 1 nsec. Subsequently it is clear that this back injection component can form a major limitation to solar cell conversion efficiency. Furthermore, its magnitude limits conversion efficiency gains as a result of high doping densities and/or geometric variations on the base p and back p^+ regions.

The selection of the lifetime values of 1 nsec and 100 nsec in the surface region are somewhat arbitrary. For lifetimes below 100 nsec the resulting calculations are quite lifetime dependent. For example. Fossom's analysis at Sandia (1975) produces results comparable to experimental data only by including a sub nanosecond surface region lifetime (no heavy doping effects). On the other hand work by Brandhorst (1975) which included heavy doping effects (via Van Overstraeton) obtained a reasonable data match with higher lifetimes but with an anomolous diffusion profile. However, virtually all of the past work in this regard must be viewed with the realization that both the lifetime and the magnitude of band gap reduction in heavily doped diffused silicon exhibit a large range of uncertainty. This, when coupled with the possibility that the effects of band gap reduction and low lifetime cannot be accurately superimposed due to interactive effects allows room for much speculation as to the dominant mechanism limiting solar cell efficiency for low resistivity cells.

It was also found that the mechanisms which limit the conversion efficiency are not the same over the entire range of proposed base resistivities. As can be seen from Figure 1.1 low surface region lifetime has little effect upon higher resistivity solar cells (greater than 10 ohm-cm). The major factors which come into play in this range are high injection phenomena both at the injecting and reflecting junction. For reasons such as this, the picture of solar cell operation has been broken down into three fairly distinct regions based upon base resistivity. The low resistivity region (below about 1 ohm-cm) can be characterized by phenomena such as band gap reduction due to heavy doping effects in the surface region and short diffusions lengths both in the surface and base regions. These have major consequences in the surface region and reduce the conversion efficiency to below what is obtained by the usual first order analysis. On the other hand there is a high resistivity region (above about 10 ohm-cm) where these same phenomena do not have significant effects. In this region, high injection effects tend to reduce the conversion efficiency to levels below that expected by first order models due to a reduction of the curve factor. In the center region of resistivity (between 1 and 10 ohm-cm) the operation of the cell is relatively simple in that it can be quite adequately described by models which include only first order mechanisms since back injection, high injection phenomena, and heavy doping effects are not significant.

It is quite convenient to break solar cell conversion efficiency down into the constituent components of open circuit voltage, curve factor, and short circuit current. The dependences of these quantities on base resistivity are illustrated in Figures 1.2 thru 1.4 respectively.

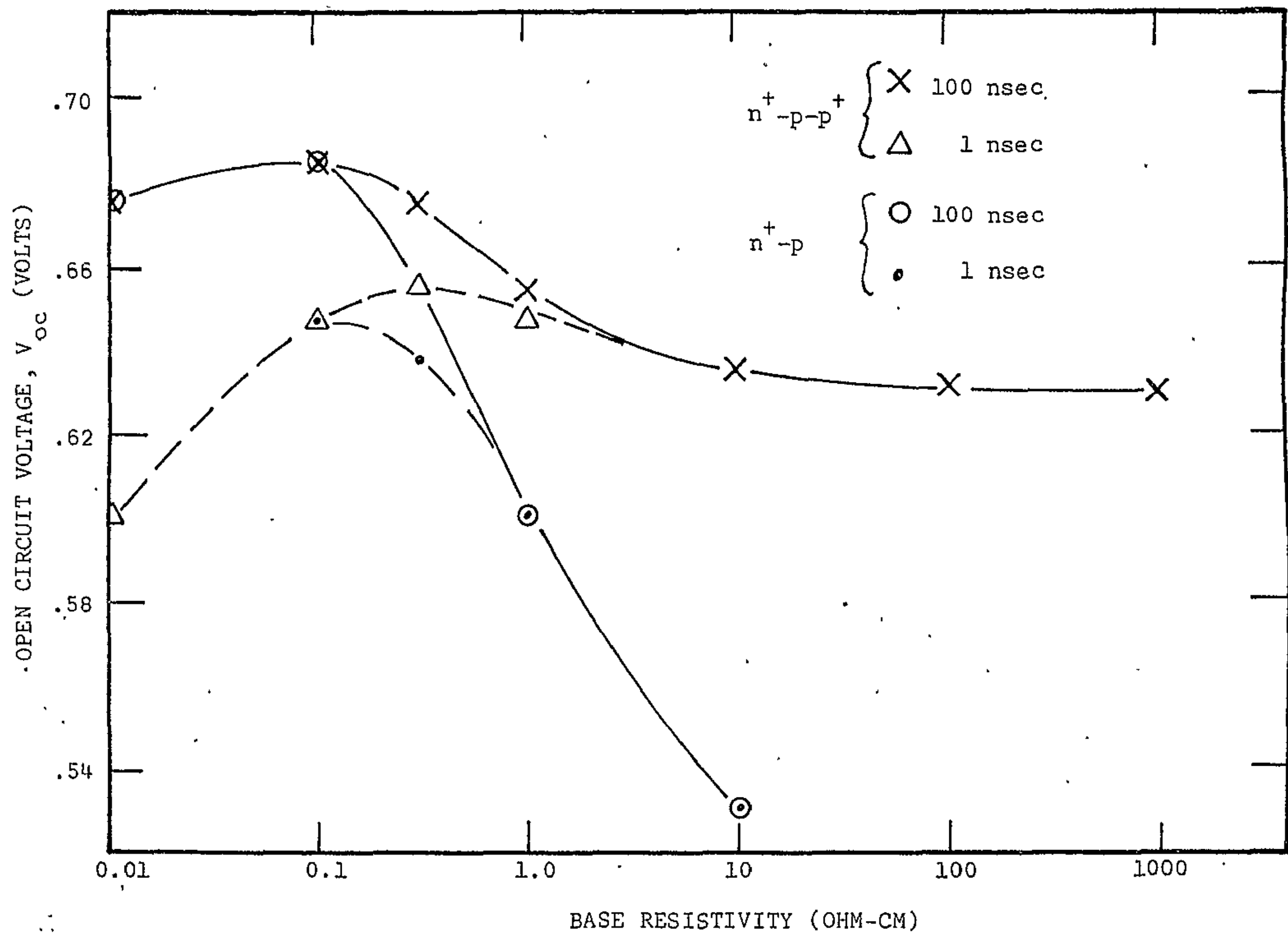

Figure 1.2 Open circuit voltage as a function of base resistivity (See Table 1.1).

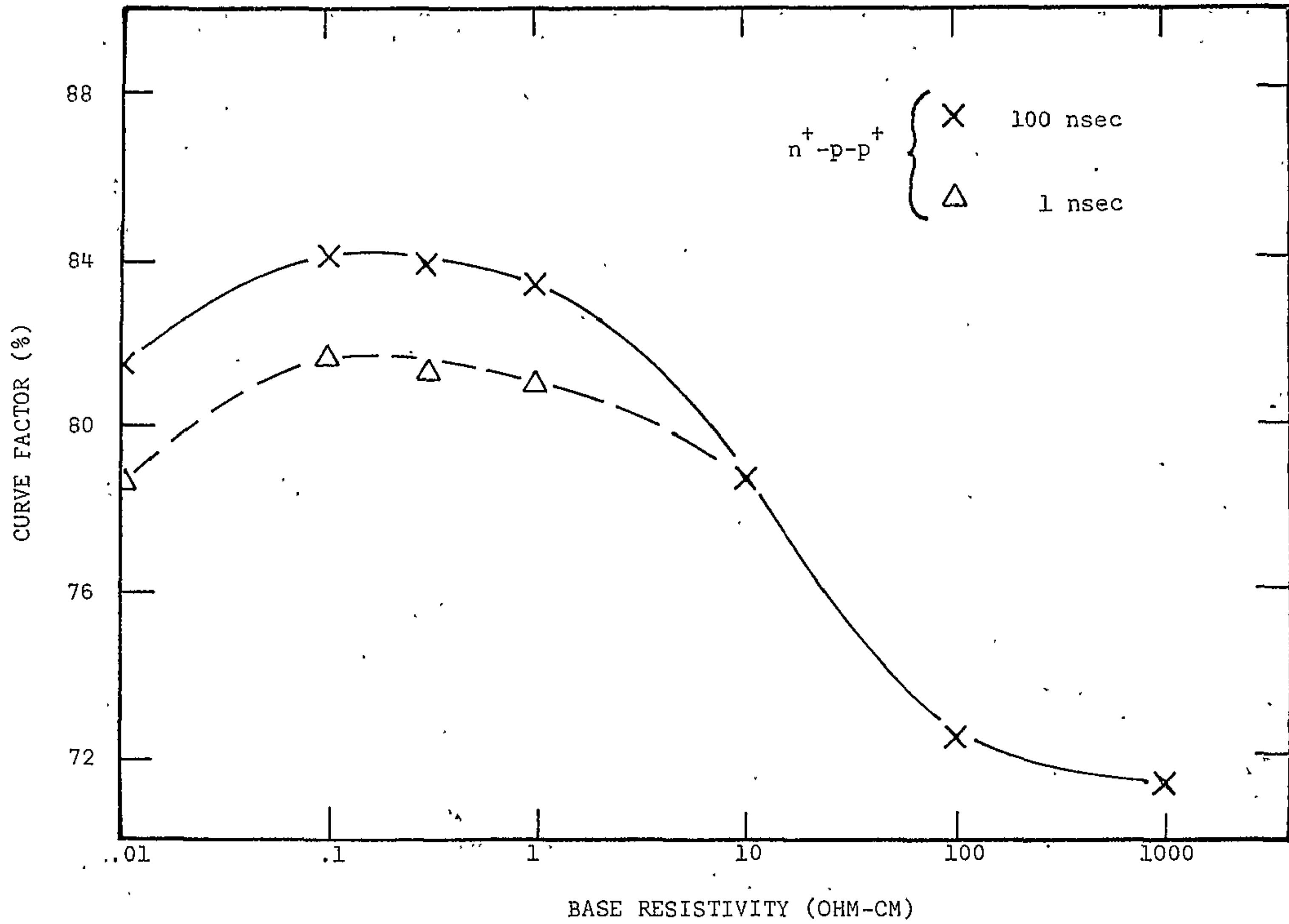

Figure 1.3 Curve factor as a function of base resistivity (See Table 1.1).

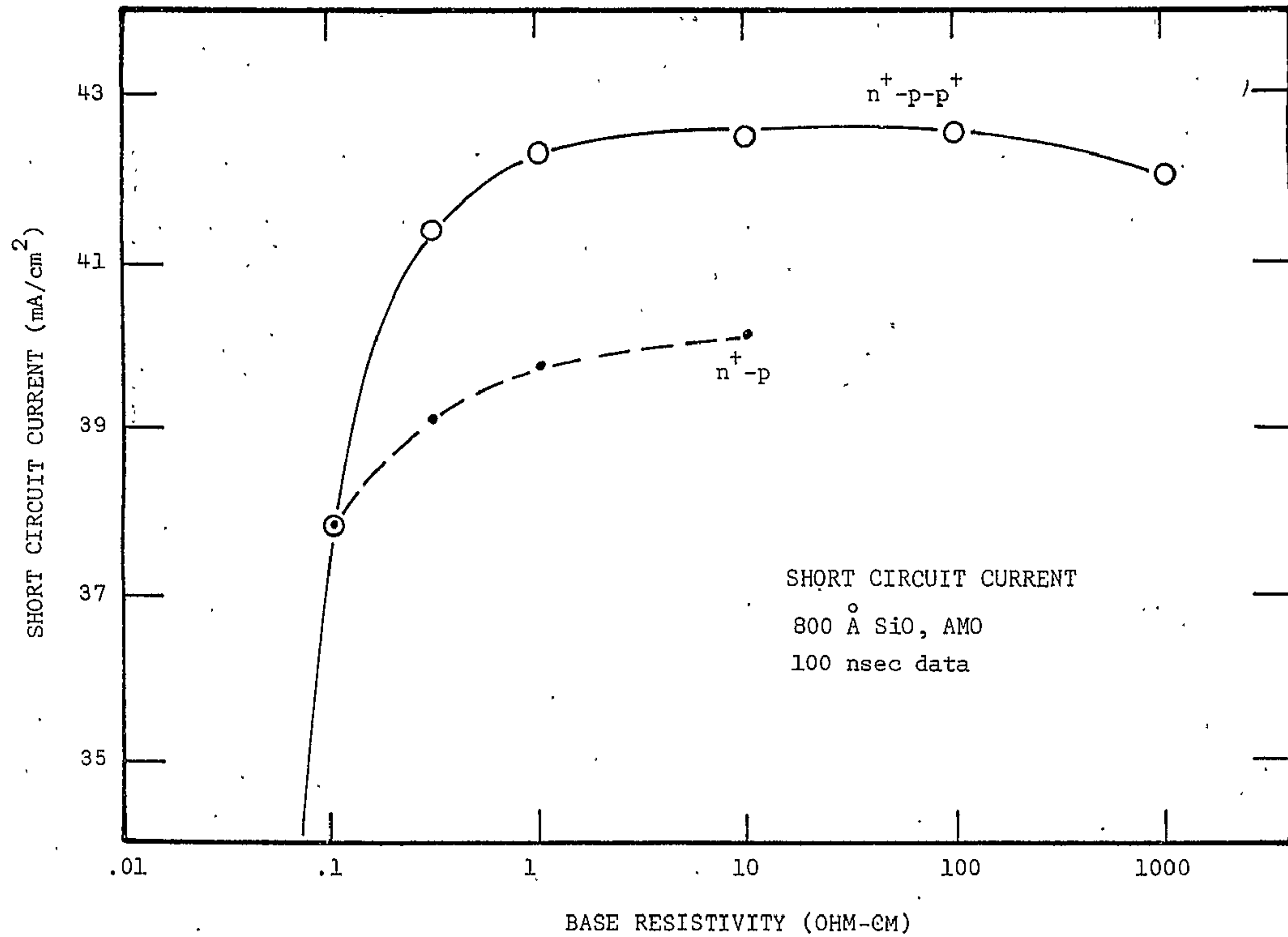

Figure 1.4 Short circuit current as a function of base resistivity (See Table 1.1)

In viewing the open circuit voltage, the three regions of operation described above are quite apparent. In the low resistivity region the open circuit voltage tends to saturate due to the predominance of the back injection component. An additional decrease is due to the reduction of the collection efficiency. The peak value of open circuit voltage is dependent upon surface region lifetime as seen in the figure. In addition, depletion region currents can become significant which tends to suppress the open circuit voltage even further. The existence of the depletion region components can be verified by the reduction in curve factor seen in Figure 1.3. The center region of resistivities is characterized by the expected dependence of open circuit voltage upon base resistivity and also relatively constant curve factors. The high resistivity region on the other hand illustrates relatively constant open circuit voltages for the n^+-p-p^+ cell but a sharp decrease in the curve factor due to high injection phenomena. Note also that there is a slight reduction in short circuit current due to resistive drops in the lightly doped center region.

Summarizing, it is seen that the most promising area for high efficiency solar cells is the low resistivity (about 0.3 ohm-cm) n^+-p-p^+ structures. However, to realize the enhanced efficiencies afforded by this structure means must be found to minimize the relative magnitude of the back injection component. Without this, further gains which can be postulated through reductions of the forward electron component will be nullified.

2. GEOMETRIC VARIATIONS

2.1 Objectives

The current state of conventional silicon solar cell design includes a realization that significant improvements in conversion efficiency will come only from increases in the open circuit voltage. Optimization of other parameters, although still possible, will not significantly improve the current solar cell (Brandhorst, 1975). Consequently the major orientation of this section is to view methods by which the open circuit voltage can be increased. Given a fairly constant short circuit current, the open circuit voltage is determined by the forward dark characteristics of the solar cell. This forward characteristic is made up of three major components, each of which must be minimized. The first of these is the injection of electrons from the n^+ surface region into the p-type base region. This component has been reduced thus far through the use of a n^+-p-p^+ structure with optimum values for base resistivity and high-low junction interaction. However, further improvements can be obtained through the narrowing of the p region width. This is the topic of the following section. The most serious tradeoff in this technique is the loss of short circuit current due to short optical path lengths. However, if total optical reflection at the back surface of the solar cell occurs, this tradeoff does not become quite as critical. This section assumes total optical reflection at the back surface through a "two pass" model. The details of the inclusion of this model are discussed in Section 3.1.

The other component of forward current is that of hole injection into the n^+ surface region from the p-type base region. Normally, due to heavy doping levels within the surface region this component can be

neglected. However, with reduced electron injection into the base layer the neglect of this back injection component is not valid. Further reductions of electron injection makes this component dominant. The back injection current component is dependent upon the lifetime and band gap shrinkage within the surface region. There is a large range of uncertainty as to the magnitude of both of these parameters. Nonetheless, a relative reduction of this current component can result from a reduction of the width of the region. Section 2.3 discusses the effects of such a reduction in width, with a particular emphasis upon improvements which may be gained for the extreme case of low surface region lifetime. Heavy doping effects are included throughout this report by means of an empirical model for band gap shrinkage [Hauser (1969)]. This model produces results between the extremes of "effective doping" as predicted by van Overstraeton (1973) and Mock (1973).

The third component of forward current is that of depletion region recombination. This component is a strong function not only of the magnitude of the lifetime but also of its spatial dependence. Subsequently, further discussion of this current component is included in the section which treats spatial lifetime models.

The cells discussed in this chapter are for the most part 0.3 ohm-cm n^+-p-p^+ solar cells. The complete information on the cells is tabulated in Table 2.1. Note that these cells include total optical reflection at the back surface and a 5 percent "non-reflecting" film. Consequently the efficiencies and open circuit voltages are somewhat higher than those of the prior chapter. The detailed information on the improvements in performance due to the two pass optical model and a nonreflective film are discussed in Section 3. Other than the optical nature of the cells,

Table 2.1. Characteristics of Solar Cells Analyzed in Chapter 2.

n^+ Region Thickness	0.25 μM
p Region Thickness	Variable
p^+ Region Thickness	5 μM
n^+ Surface Concentration	$10^{20}/cm^2$
p Region Resistivity	0.3 Ω·cm
p^+ Doping Concentration	$10^{19}/cm^3$
Lifetime in n^+ Region	100 nsec
Lifetime in p Region	65 μsec
Diffusion length in p region	340 μM
Lifetime in p^+ region	0.37 μsec
Surface Recombination Velocity	10^3 cm/sec
Antireflection Layer	"5% film"
Irradiance Conditions	AMO

the center p-type base region width, and the specification of center p-type resistivity these cells are identical to those of the past work outlined in the prior chapter.

2.2 Base Region Width

The width of the base region of 0.3 ohm-cm n^+-p-p^+ solar cells was varied to determine the effect of such a variation on the overall conversion efficiency. A high lifetime in the n^+ surface region was selected in order to minimize the effects of back injection into the n^+ surface region so that optimization of the conversion efficiency based upon the resulting reduction of electron injection into the center p-type base region could be isolated.

Figure 2.1 indicates the resulting dependence of the total forward dark current at 0.7 v forward bias upon the center region width. As expected, the total current decreases with a decrease in region width. The first order analysis indicated in the figure neglects hole injection into the surface region and depletion region current. However, if these current components as calculated from the complete analysis are added to the first order results, a more reasonable match is obtained as shown by the dashed curve. Nonetheless, the exact analysis still indicates not only a larger current density but also a non-linearity. This could be due to the methods by which center region recombination and high-low junction reflection are approximated in the first order methods. However, these first order results follow very closely those of Godlewski (1973) whose methods of including base recombination are quite accurate. At 0.7 v forward bias, the magnitude of the total hole current flowing into the surface and depletion region amounted to 18 mA/cm^2. This value is independent of p region width. It should be realized that these results

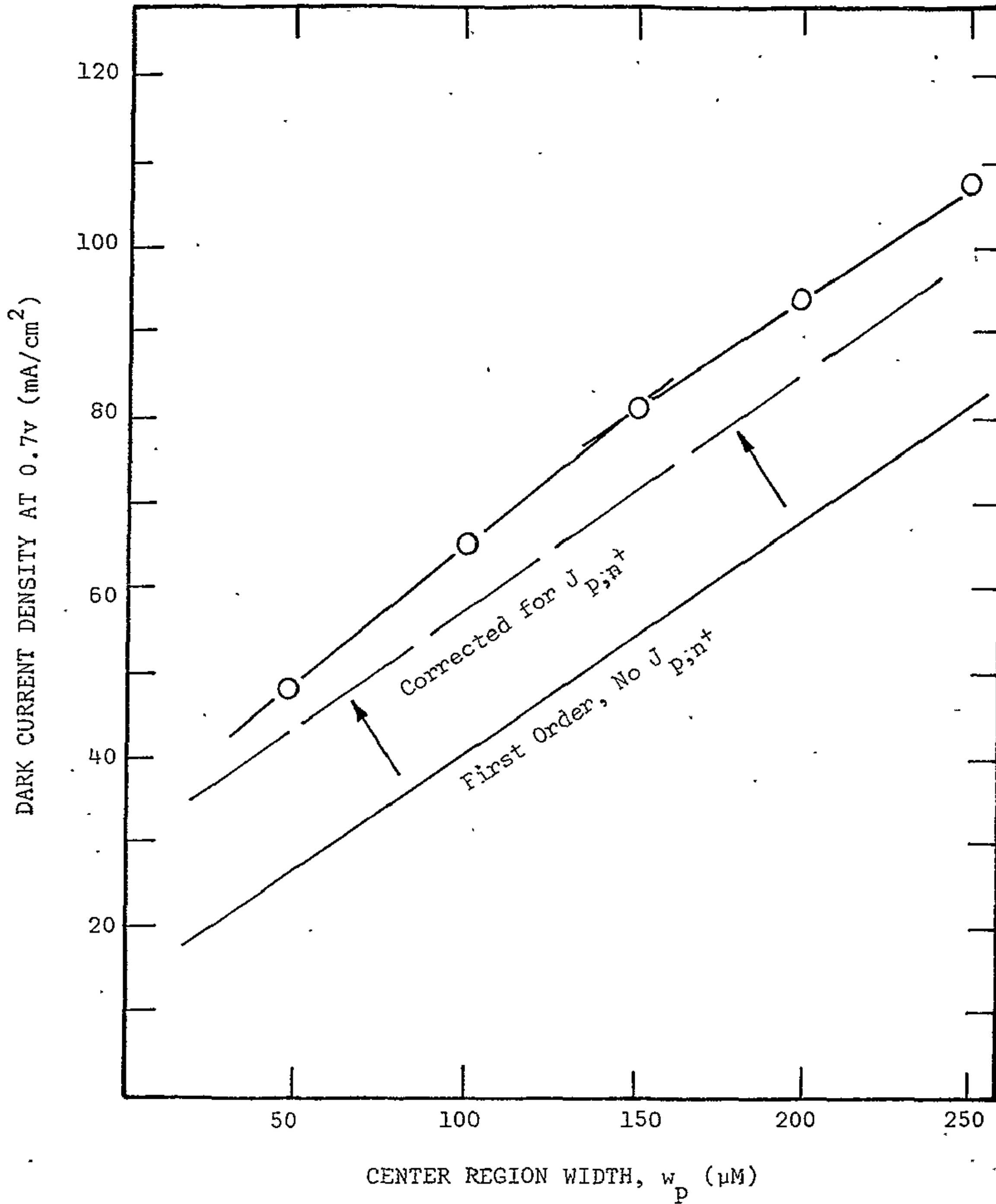

Figure 2.1 Total forward dark current density as a function of center region width (See Table 2.1).

are for a rather ideal n^+ surface region in that the lifetime is taken as a constant 100 nsec. Even under these conditions this current component is significant.

Figure 2.2 illustrates the dependence of the open circuit voltage on p region width for these cells. As expected, the open circuit voltage increases with decreasing device width. However, the values are below what is expected from first order analysis (dashed curve) due again to the neglect of the injection of carriers into the surface region and the n^+-p depletion region current. However, as can be seen from the figure, the curve resulting from a correction due to those hole components, the magnitudes of which are obtained from the complete analysis, is still more optimistic that the complete analysis. This is the same discrepancy seen in the prior figures regarding the dark characteristics.

Figure 2.3 illustrates the resulting conversion efficiencies for these solar cells. As can be seen, the efficiency peaks at a cell thickness of about 150 μM. The reduction of efficiency at the wider device lengths is due to the reduction in open circuit voltage. The diffusion length for this base resistivity is taken as 340 μM indicating that recombination effects should not be appreciable in this range of base widths. At narrower base region widths the reduction in efficiency is due primarily to the reduction in short circuit current. The decrease in efficiency for very narrow base widths however may not be as severe in actual devices as indicated by Figure 2.3 since the model utilized does not include additional photon passes due to internal reflection at the irradiated surface.

The results of first order models are also illustrated in Figure 2.3. These were calculated using curve factors of 0.84. This value

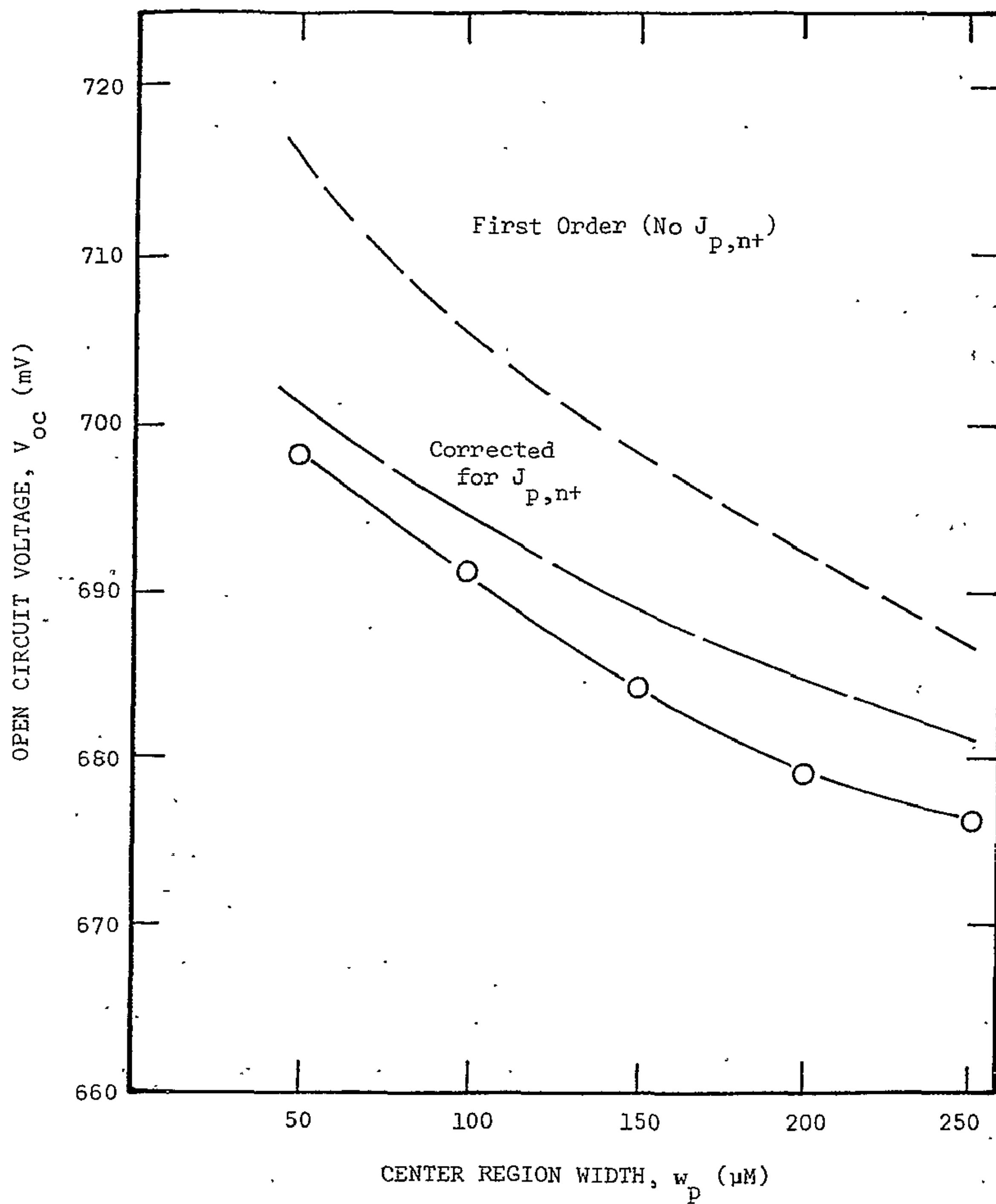

Figure 2.2 Open circuit voltage as a function of center region width (See Table 2.1).

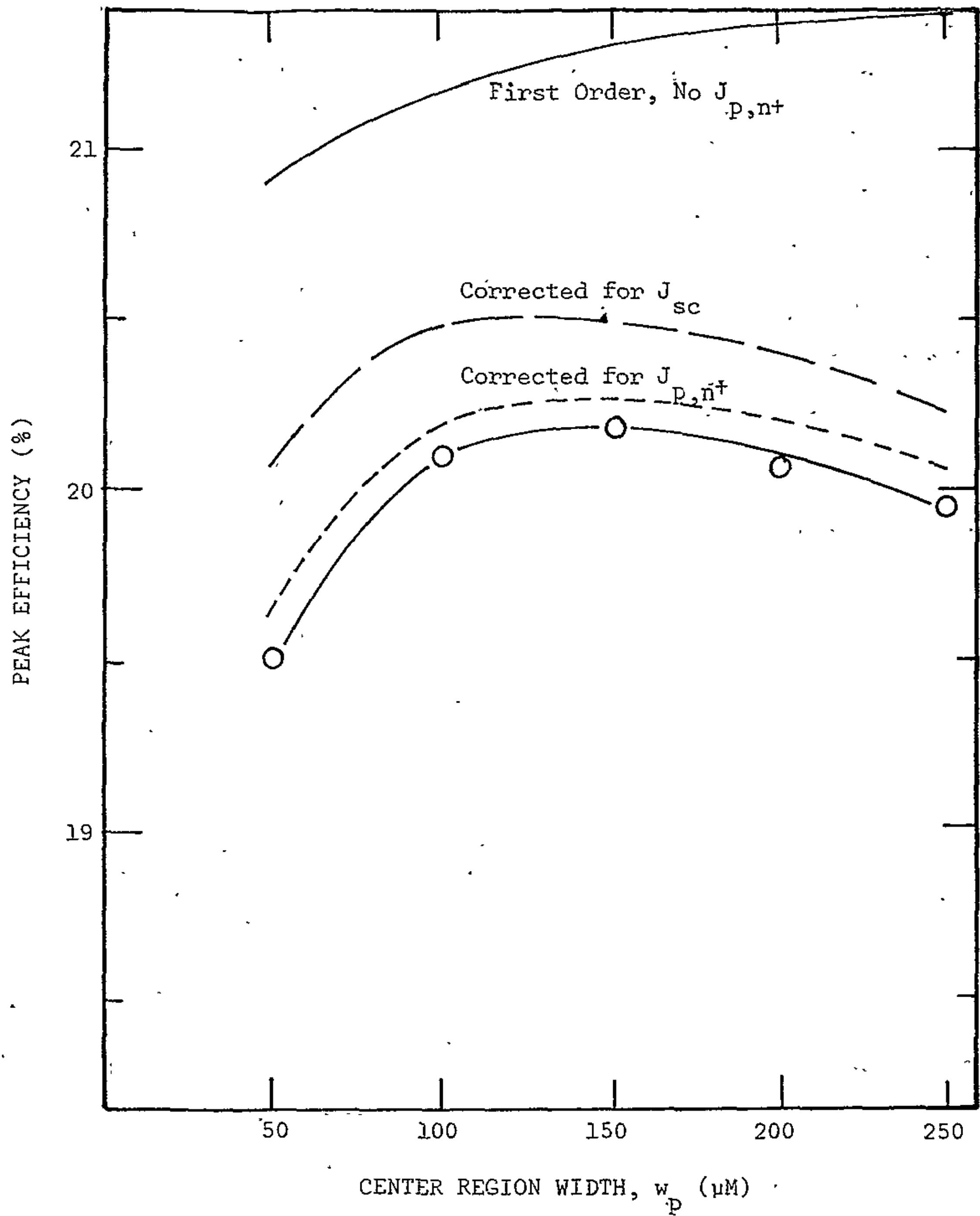

Figure 2.3 · Conversion efficiency (AMO) as a function of center region width (See Table 2.1).

agrees quite well with the exact value which did not change significantly over the range of device widths studied. The overall discrepancy between the two sets of results is twofold. For one, the first order model for the short circuit current as a function of device width neglected recombination and diffusion effects due to the non-linear generation rate. Using the results of the complete analysis to correct for this, results in the corrected curve marked in the figure. Secondly, the first order model neglected hole currents injected into the surface region. Again using the results of the complete analysis to correct for this effect, it can be seen that very close agreement is obtained. Subsequently it can be concluded that narrow base region n^+-p-p^+ solar cells with back surface reflectance can be fabricated without any loss of conversion efficiency. Recent work by Michel _et al._ (1975) confirm the conclusions made in this section.

2.3 Surface Region Widths

The prior section discussed improvements possible in solar cell performance by a reduction of the electron injection into the center p-type base region. However, that work was performed with an n^+ surface diffused region which was optimistically characterized with respect to lifetime. With a non-optimum lifetime characterization _i.e._ 1 nsec, there is a sharp reduction in open circuit voltage and consequently the overall efficiency due to the dominance of hole injection into the n^+ surface diffused region. Subsequently this section discusses the reduction of this hole component through a narrowing of the surface region width. For the most part calculations are made for the low lifetime case since a modification of the region width has little effect for the higher lifetime case. In addition, the cells studied are those

of 100 μM center base region width since this produces an optimum case as discussed in the prior section. Thus the cells have the characteristics of Table 2.1 except for surface region lifetime (1 nsec), center region width (100 μM), and surface region width (variable).

Figure 2.4 illustrates the total value and hole component of dark forward current density as a function of n^+ region width. Also included in the figure is comparison data for the same cells with a 100 nsec region lifetime. From this it can be seen that the n^+ region width reduction results in a substantial reduction in the hole current density for the low lifetime case but very slight reductions for the high lifetime case. These significant reductions have direct effects upon the open circuit voltage as seen from Figure 2.5. The point of major interest is that narrow surface region widths can be effective in compensating for the effects of low surface region lifetime.

Figures 2.6 and 2.7 illustrate the dependence of short circuit current and curve factors upon the region width. The increase in the curve factor could be due to a reduction of the depletion region current component as the diffused region width is narrowed. This would occur for a constant surface concentration since the n^+ depletion region width would be narrowed. This cannot be readily verified quantitatively since there is no well defined depletion region edge in the exact simulation.

The resulting efficiencies of these cells is illustrated in Figure 2.8. These results make it quite apparent that the reduced width can be effective in increasing efficiency for the low lifetime case. However, for n^+ region lifetimes below 1 nsec, the surface region width necessary to produce signigicant changes may be prohibitively narrow for contemporary processing capabilities.

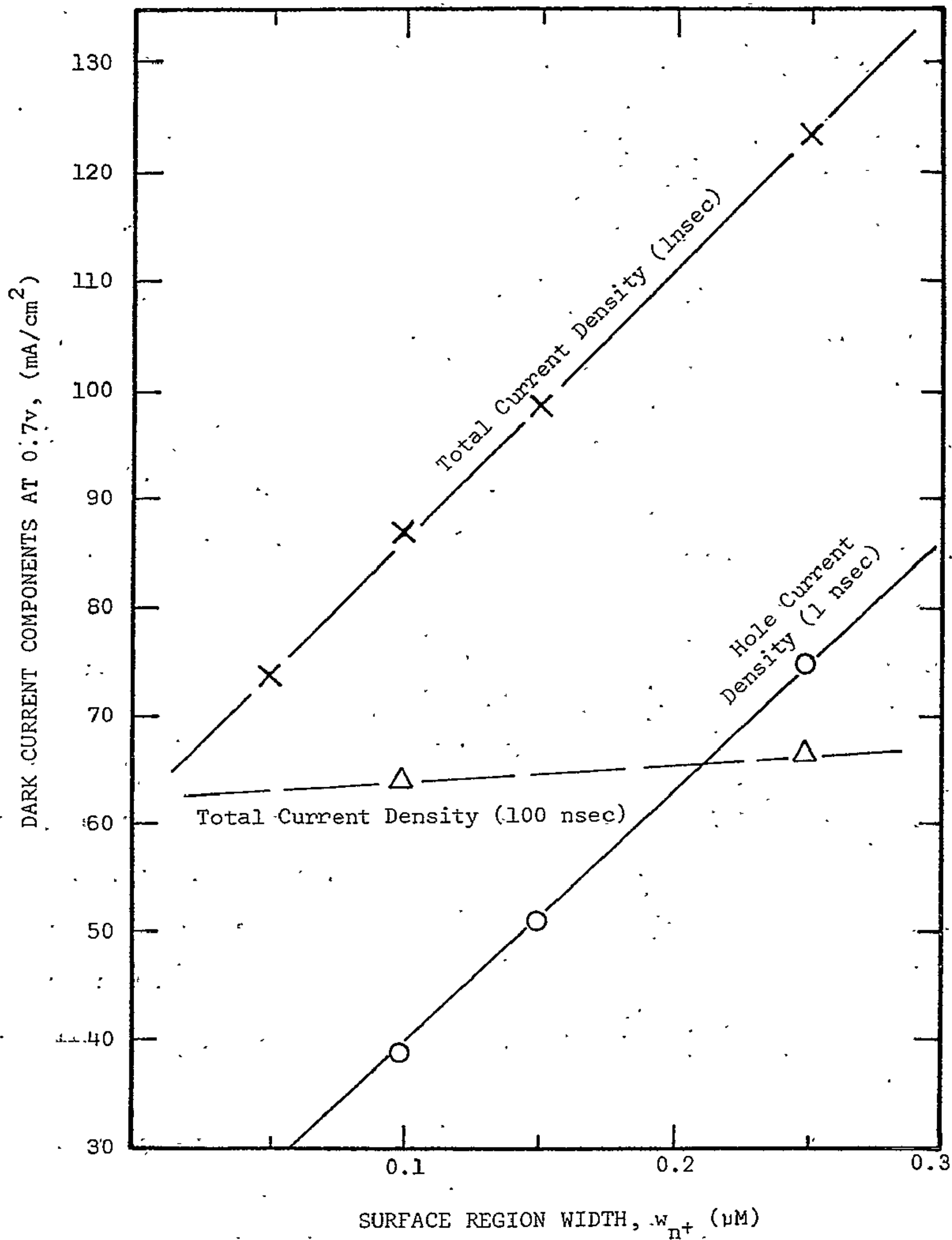

Figure 2.4 Components of dark forward current density as a function of diffused region width (See Table 2.1; variable n^+ region thickness, p region thickness of 100 μM, and n^+ region lifetime of 1 nsec or 100 nsec).

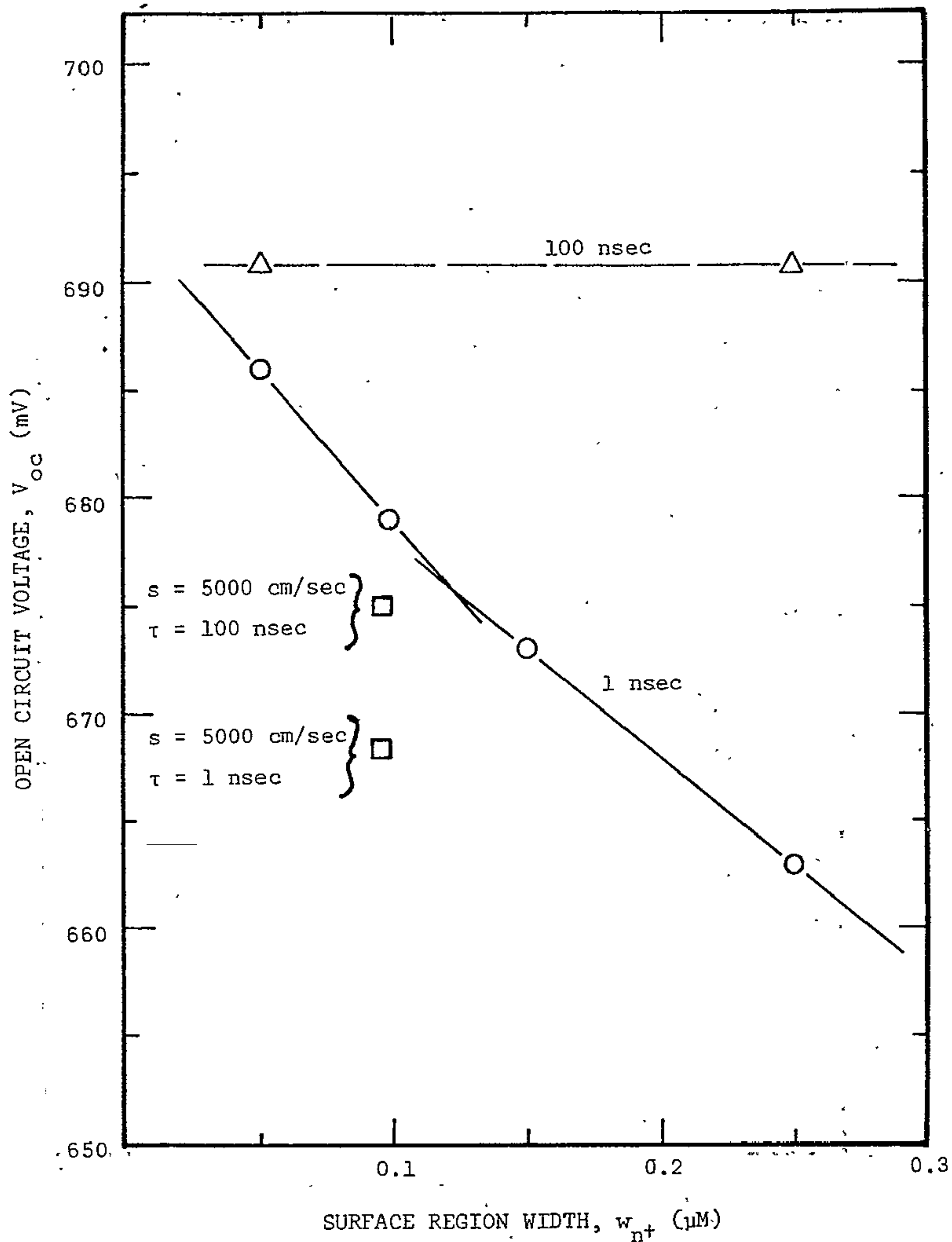

Figure 2.5 Open circuit voltage as a function of diffused region width (See Table 2.1; variable n^+ region thickness, p region thickness of 100 μM, and n^+ region lifetime of 1 nsec or 100 nsec).

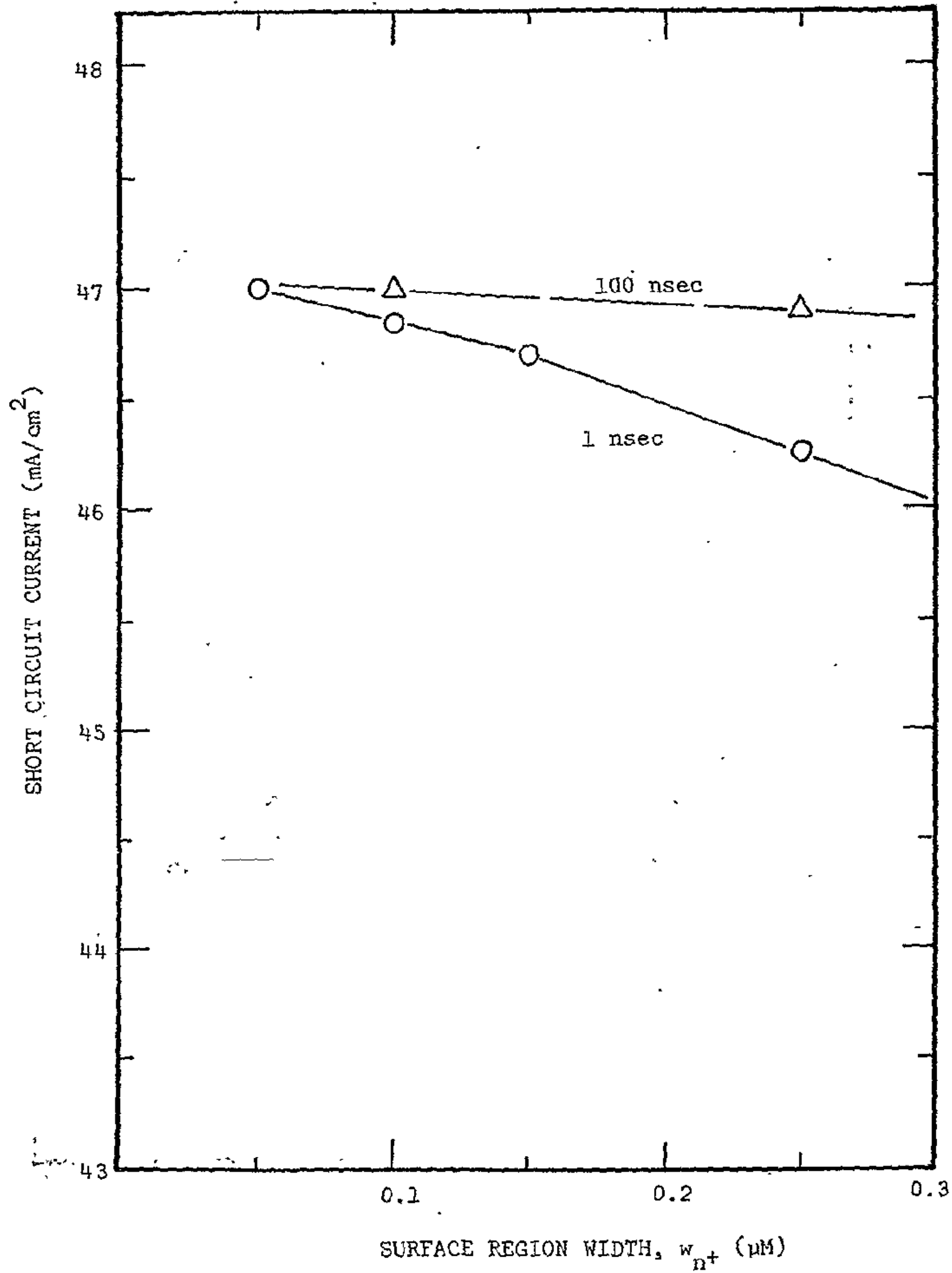

Figure 2.6 Short circuit current as a function of diffused region width (See Table 2.1; variable n^+ region thickness, p region thickness of 100 μM, and n^+ region lifetime of 1 nsec or 100 nsec).

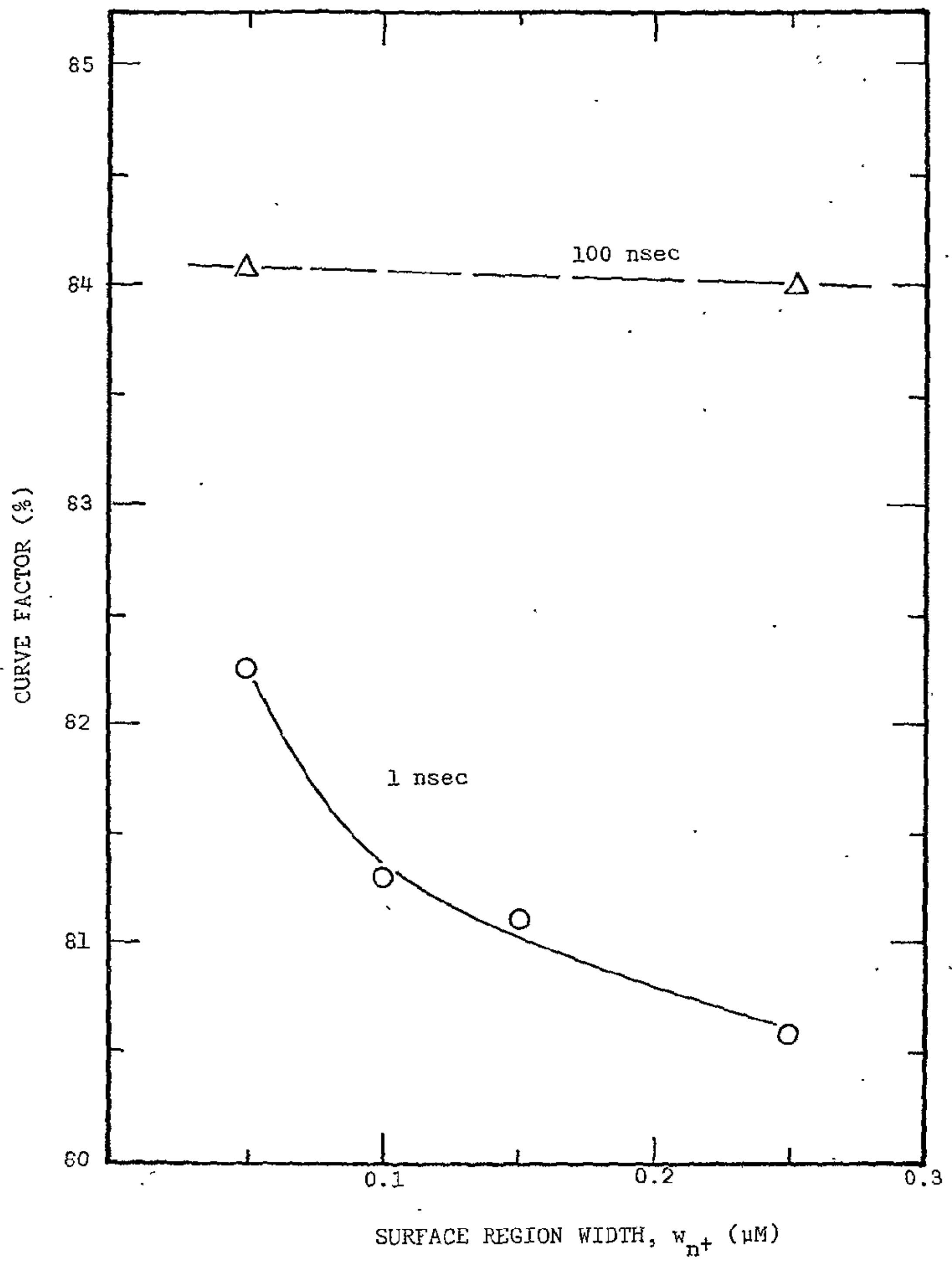

Figure 2.7 Curve factor as a function of diffused region width (See Table 2.1; variable n^+ region thickness, p region thickness of 100 μM, and n^+ region lifetime of 1 nsec or 100 nsec).

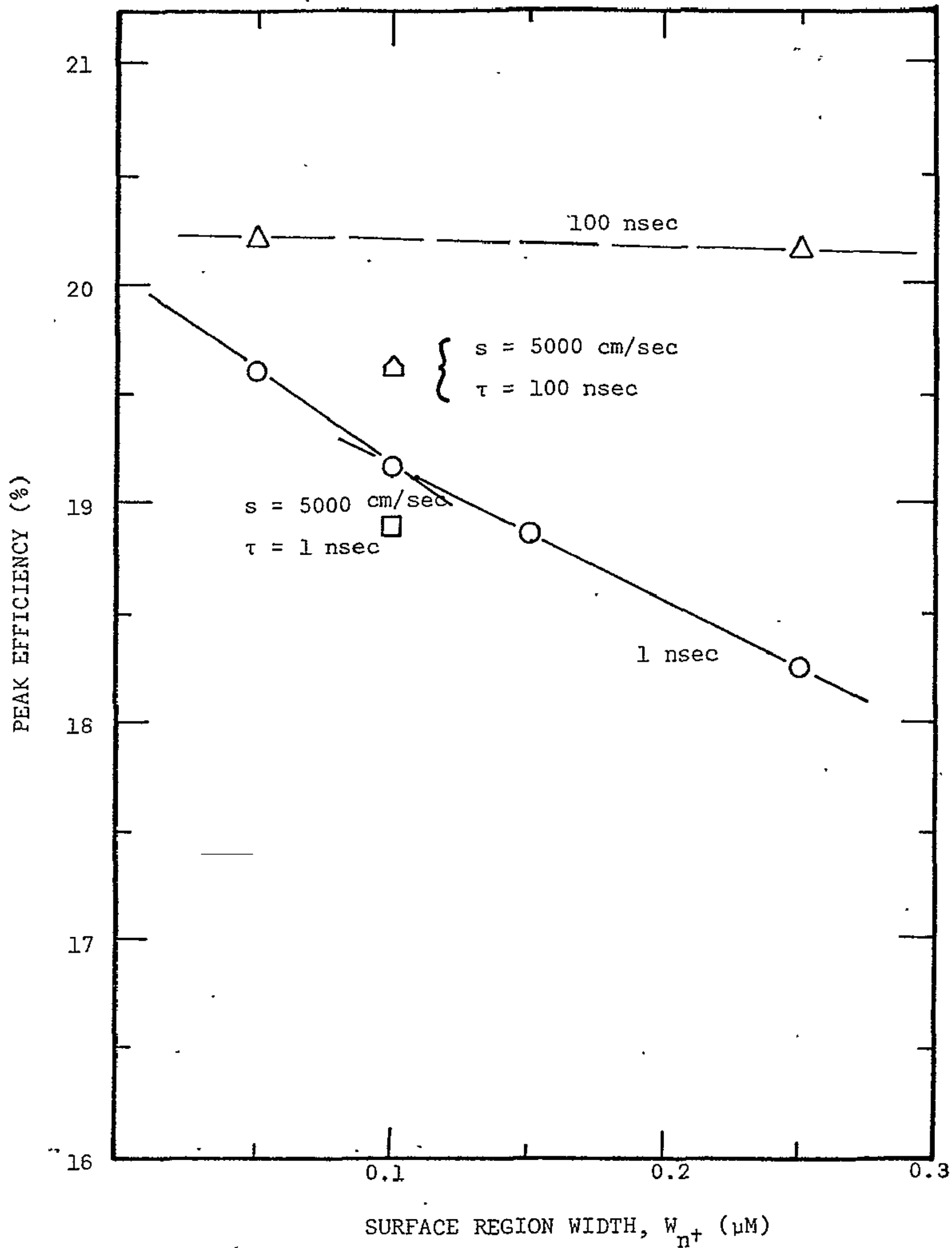

Figure 2.8 Conversion efficiency as a function of diffused region width (See Table 2.1; variable n^+ region thickness, p region thickness of 100 μM, and n^+ region lifetime of 1 nsec or 100 nsec).

All of the prior results were performed with a surface recombination velocity of 1000 cm/sec. However with a narrow surface region the dependence of the results on this parameter becomes more critical. For example Figures 2.5 and 2.8 indicate the effects of raising the surface recombination velocity to 5000 cm/sec (isolated data points). It can be seen from Figure 2.8 that there is a larger reduction in conversion efficiency for the higher lifetime case due to the large diffusion lengths in the surface region.

The results for this section are based upon a constant n^+ region lifetime. Somewhat different conclusions can be reached if a lifetime model which varies spatially in the n^+ region is used. These are discussed in a later section.

2.4 Other Surface Profiles

In relationship to hole injection into the surface region, two modifications to the surface region profile were considered. More detailed profile changes are discussed in a later section. However, an interesting modification is to select the surface concentration so that these is no retrograde field within the diffused region due to band gap reduction phenomena (Godlewski, 1973). For the heavy doping model used in this work, the surface concentration required to do this is $2 \times 10^{19}/cm^3$. Furthermore, this was attempted on the structure which had the minimum back injection current component. The structure was that of the n^+-p-p^+ configuration listed in Table 2.1 with the narrow (0.1 μM) n^+ surface width. However, the removal of the retrograde field by this method did not have significant effects upon the efficiency. Although there were slight increases in the open circuit voltage and the short circuit current for the low lifetime case, there was a reduction in the curve factor due to a wider depletion region in the n^+ side of the junction.

The second profile studied was that of a uniform surface region. The assumption behind this selection is that the lifetime within the uniform region can be taken from the data of Iles for bulk silicon. This results in a lifetime of around 200 nsec for a doping level of $2 \times 10^{19}/cm^3$. Although the actual lifetime may not be that high, it would probably be higher than that of a diffused region of $2 \times 10^{19}/cm^3$ surface concentration and 0.1 μM in width. This calculation, again with the cells of Table 2.1 with a 0.1 μM n^+ region, did not result in very significant gains. The slight improvement which did exist was due to increases in the open circuit voltage. Nonetheless, the efficiency did not decrease, leading to the conclusion that the doping dependent fields in thin diffused surface regions are not as significant as previously expected.

3. ANTIREFLECTION FILMS

3.1 Back Surface Reflection

As presented in the previous sections, gains in conversion efficiency can be obtained if the overall device thickness is narrowed when total optical reflection from the back surface of the solar cell is assumed. Since this is a potentially feasible manufacturing process and may also occur due to internal reflection in textured surface cells such as the COMSAT CNR cell, a "two pass" model was developed in the simulation program.

Since the simulation involves the solution of the basic semiconductor device equations including a spatially dependent generation rate term, the two pass model is based upon a linear addition of incident and reflected generation rates. Essentially, a subsidiary program calculates the spatial dependence of a generation rate in silicon material which is twice the width of the solar cell considered. The main simulation program then "folds" the generation rate quantities back for spatial values greater than the device width and adds these quantities to the incident generation rate at each spatial point. Since the main simulation includes the total generation rate itself, high injection levels, diffusion, etc. are still included in the overall modeling process as before.

For the wider devices (250 μM base region) the two pass model had only a slight effect, raising the short circuit current about 1.75 per cent. The efficiency reflected the same percentage increase. However, for the narrow devices (100 μM base region) the increase in short circuit current was 3.75 per cent with just under a 4 percentage increase in conversion efficiency. These increases represent a pessimistic case since the model does not include additional photon passes due to internal reflection at the irradiated or Si-AR interfaces. However, any increases due these additional

passes would be significant only for very narrow devices (base region widths below 100 microns).

3.2 Non-Reflective Antireflection Coatings

There has been recent emphasis and work on the textured surface or non-reflective antireflection layers. The essential characteristics of such a surface is a low, nearly constant value of reflectance ranging from 3 to 5 per cent across the wavelength range. Subsequently, the generation rate for many studies has been calculated assuming an antireflection film of constant 5 per cent reflectance. The comparisons of the results of this film with other films is tabulated in Table 3.1. A significant increase in the available optical current can be seen. The inclusion of the resulting generation rate with the exact simulation resulted in a percentage increase in efficiency of about 13 per cent over that of an optimum SiO film. This almost exactly matches the percentage in available optical current as given in Table 3.1.

In the fabrication of a typical textured surface, the junction follows the texture of the surface. Consequently a correction should be made in any one-dimensional calculation to dark current due to the increase in junction area. For a pyramidal structure of base length L and an apex angle of 70.5°, the total surface area is $1.74\ L^2$. Thus, the current component injected into the surface region must be increased by the factor 1.74. This factor however does not produce a significant decrease in the open circuit voltage due to its logarithemic dependence upon the dark current density.

3.3 Other Antireflection Films

Due to the short wavelength light absorption in thin SiO films, several other films have been suggested for use as solar cell antireflection layers. These include SiO_2, Ta_2O_5, Si_3N_4, TiO_2, Nb_2O_5, HfO_2, and ZrO_2. Data on some

Table 3.1. Summary of Excess Carrier Generation in Silicon

Geometry	Spectral Conditions	Optimum Anti-Reflection Thickness (Å)	Surface Loss[a] (%)	Available Optical Current[a] (mA/cm^2)	Surface Generation Rate[a] (#/cc/sec)
Si	AMO	N. A.	36.4	34.2	1.15×10^{22}
	AM2	N. A.	34.7	22.4	1.62×10^{21}
Si + SiO	AMO	800	15.6	45.4	5.96×10^{21}
	AM2	800	10.4	30.7	1.39×10^{21}
Si + SiO_2	AMO	1100	17.6	44.3	1.25×10^{22}
	AM2	1100	14.5	29.3	1.83×10^{21}
Si + "5% Film"	AMO	N. A.	5.0	51.1	2.71×10^{22}
	AM2	N.A.	5.0	32.6	3.14×10^{21}
Ta_2O_5	AMO	720	12.5	47.0	1.56×10^{22}
	AM2	720	9.5	31.1	1.89×10^{21}

[a]Computed at optimum antireflection thickness if applicable.

of these films has been presented by Wang et al. (1973) which indicated that multilayer SiO-TiO_2 films produced improved results over SiO-Ta_2O_5 multilayers. However, these calculations neglected the absorptance in both the SiO and TiO_2 layers. Work by Travina and Mukin (1966) and others indicates that TiO_2 is lossey in the short wavelength region. In addition, the properties of TiO_2 are very process dependent, with the index of refraction ranging from 2.2 to about 2.9 (See Heitman, 1971). Subsequently there has been a major interest in Ta_2O_5 antireflection films since the film does not begin to absorb light until below 0.3 μM wavelength (Knausenberger and Tauber, 1973). The index of refraction is close to an optimum value, although its value is also process dependent (Revesz, 1976).

A detailed analysis was performed with the Ta_2O_5 films. Part of these results are listed in Table 3.1 which indicates an optimum thickness of 720 Å. The index of refraction data for the analysis was taken from the data of Young (1958). Figure 3.1 illustrates the reflectance and transmission coefficient resulting from an optimum layer. This data is quite similar to that calculated by Wang et al. (1973) and measured by Revesz et al. (1976) for wavelengths greater than 0.3 μM. The data indicate an improvement over an optimum SiO film with respect to available optical current. The complete analysis indicated an improvement in short circuit current of about 4 per cent. Measured data by Brandhorst (1975) indicated a 6 per cent increase in short circuit current with a Ta_2O_5 antireflection layer as opposed to a SiO layer. This improvement however occurred after the addition of a cover glass. Prior to this treatment the SiO film indicated a slight increase in short circuit current over the cell with Ta_2O_5.

Other films of interest include Nb_2O_5. This film however is reported to be virtually identical to Ta_2O_5 (Revesz, 1973). Another film of interest

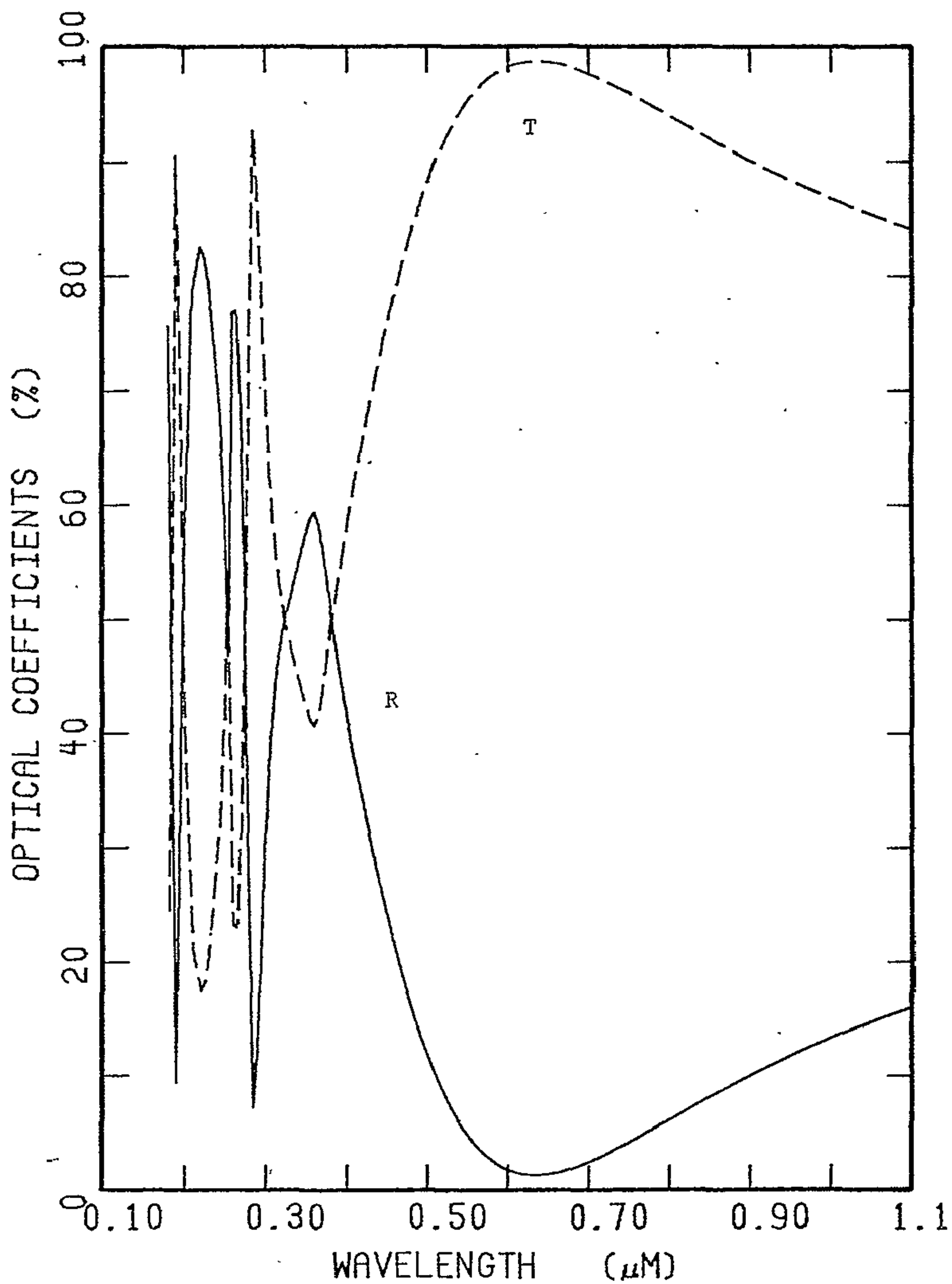

Figure 3.1 Optical coefficients for an optimum thickness of Ta_2O_5 antireflection film.

is that of ZrO_2. This film has a dielectric constant of 2.1 with an absorption edge of about 0.2 microns. However, no data was found regarding the wavelength dependence of the index of refraction. A similar situation exists for HfO_2, which has a nominal index of refraction of 2.3 (Revesz, 1973). In view of the lack of data on the wavelength dependence of the index of refraction for various films, calculations were made to determine the optimum value for the index of refraction assuming no dependence on wavelength. This was formed by evaluating the photon transmission efficiency of various thicknesses of such a film upon a silicon substrate. The silicon was fully characterized as to the wavelength dependence of both the real and imaginary parts of the index of refraction. The results of such a calculation are illustrated in Figure 3.2 which displays the photon transmission efficiency at optimum film thickness (and the optimum film thickness) as a function of the index of refraction. The peak is seen to occur at an n value of 1.95. This is somewhat below the optimum value of 2.3 reported by Revesz <u>et al</u>. (1976). However, their value was obtained by "tuning" the optical system, including a cover glass (n = 1.45) at a 0.54 micron wavelength and does not take into account the wavelength dependence of the optical properties of silicon.

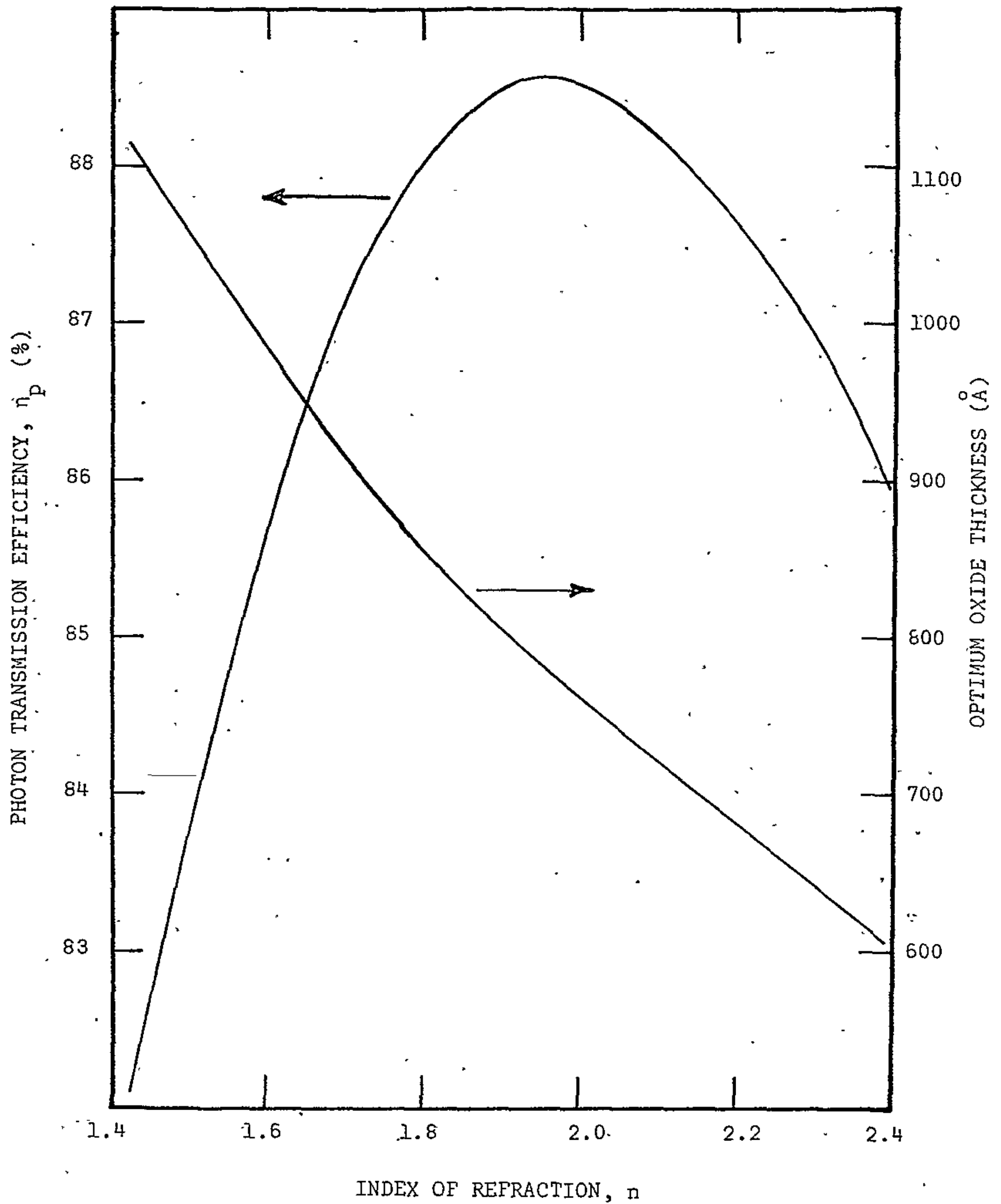

Figure 3.2 Photon Transmission efficiency and optimum thickness of a single layer, non-absorbing anti-reflection layer.

4. THE P^+-N-N^+ STRUCTURE

4.1 Primary Differences in p^+-n-n^+ and n^+-p-p^+ Structures

Most of the prior work with solar cell analysis and fabrication has involved the n^+-p-p^+ structure. Consequently there remains the question of possible differences if the structure is changed to the p^+-n-n^+ structure. Several differences in the two structures can be noted which may contribute to any such differences:

a) In the heavily diffused surface region the amount of band gap shrinkage and penetration of the Fermi energy into the conduction band differs for p-and n-type doping. This was discussed in the prior grant report and is discussed further in the following chapter. In general, heavy doping effects are not as severe in a p region as in a n region. This would tend to reduce the amount of back injection in a p^+-n-n^+ structure.

b) In the base region, the results are quite dependent upon diffusion length selected. If equal diffusion lengths are selected for both n-and p-type base regions then an n-type base region will have a higher lifetime than a p-type region due to differences in hole and electron mobility. This can effect the magnitude of the forward dark injection component with the n^+-p-p^+ structure illustrating higher values and subsequently lower open circuit voltages.

c) A Dember type potential in the base region due to the non-linear generation rate aids in the collection of short circuit current for a p-type base region and opposes the collection in a n-type base region. This however is not a major factor as discussed in the prior grant report.

The sections which follow present results for solar cell efficiency as a function of base resistivity and base region width. A concluding section discusses the lifetime dependence and gives a direct comparison to the n^+-p-p^+ structure.

4.2 Efficiency as a Function of Base Region Resistivity

The dependence of solar cell efficiency upon base resistivity is quite strong if the injection of carriers into the surface region is neglected. As discussed in the prior grant report, three major regions of operation are encountered as the base region resistivity is changed. To investigate these effects with the p^{+}-n-n^{+} structure, a high (100 nsec), constant lifetime was selected for the surface region. In this case, the efficiency is determined by the nature of the base region.

The devices analyzed include heavy doping effects, optical reflection at the back contact, a high—low junction, and a 5 per cent antireflection layer. The lifetime in the base region as a function of base resistivity is taken from the data of Iles. Other characteristics of these cells are tabulated in Table 4.1.

Figure 4.1 illustrates the dark characteristics of these devices for base resistivities ranging from 10 to 0.01 ohm-cm. As can be seen, 10 ohm-cm p-type base regions tend to show substantial high injection effects. This is due to the lighter p-type doping required to obtain 10 ohm-cm material as compared to the n-type doping. As expected, the forward current density reduces as the base resistitivy is lowered. For the 0.01 ohm-cm device the depletion region current component has increased dramatically due to the reduction of the base region lifetime. This is illustrated by the large increase in current for this device at low voltages in Figure 4.1. Figure 4.2 illustrates the illuminated characteristics of these same cells. Again it can be seen that the limiting factor with regard to low resistivity base regions is the dependence of the collection efficiency upon the base region lifetime. This conclusion can be made due to the high surface region lifetime. A lower than 100 nsec surface region lifetime would exhibit severe reductions in open circuit voltage. This is discussed in the following chapter

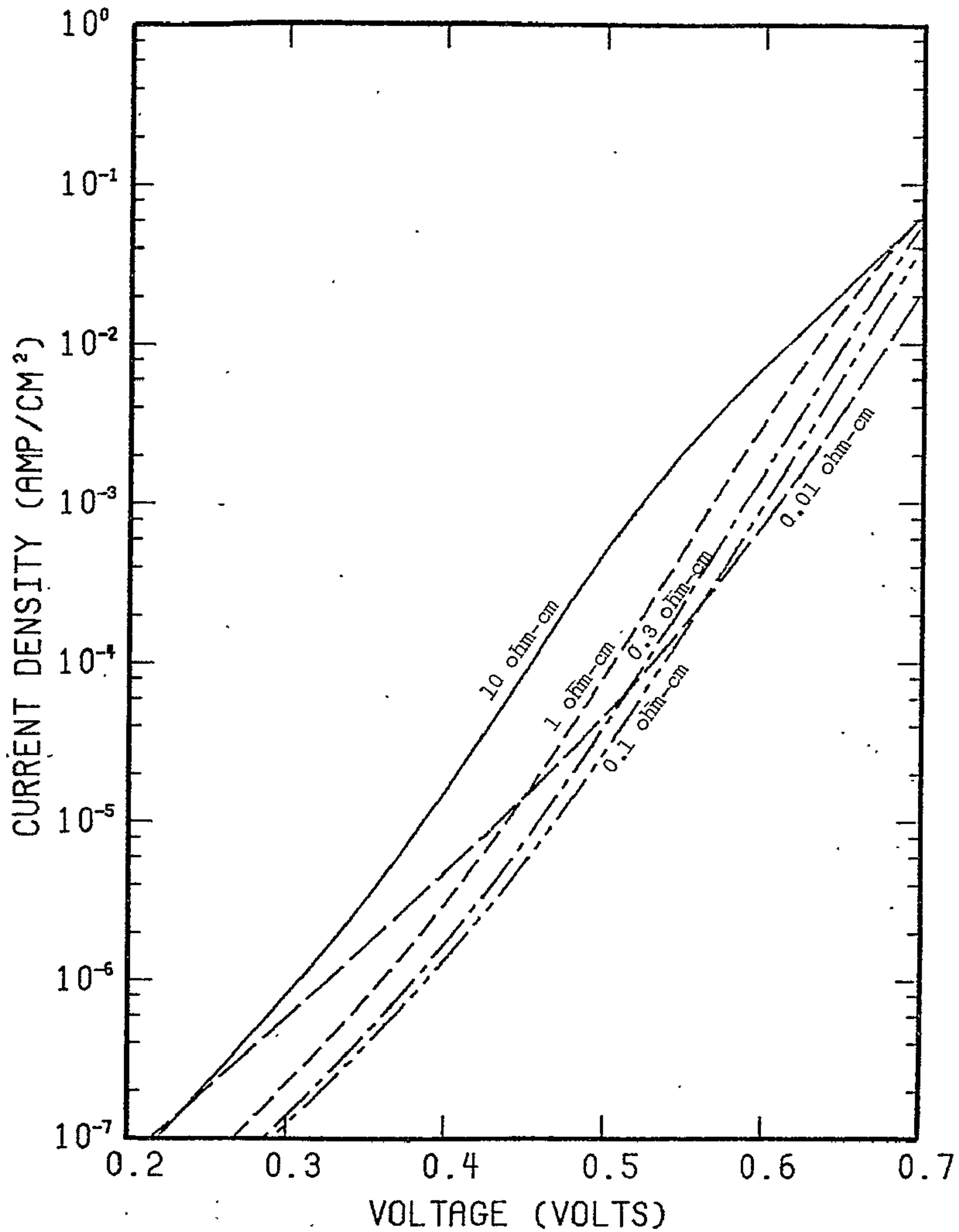

Figure 4.1 Dark characteristics of p^+-n-n^+ silicon solar cells (See Table 4.1).

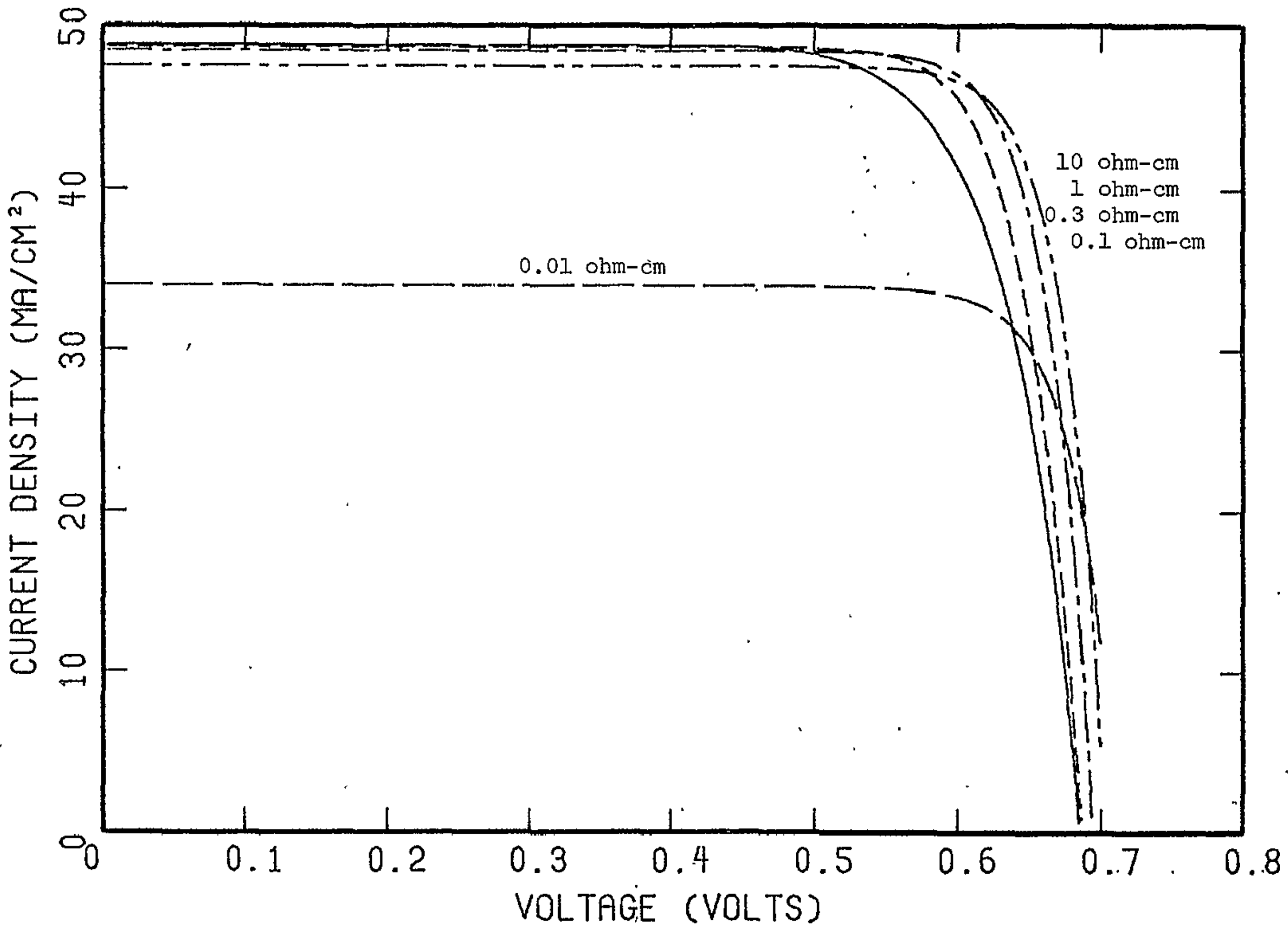

Figure 4.2 Illuminated characteristics of the p^+-n-n^+ solar cells of Figure 4.1 (AMO).

Table 4.1 Material and Dimensional Parameters of the p^+-n-n^+ Solar cells analyzed in Chapter 4

Overall Cell Thickness	250 μM
p^+ Thickness	0.25 μM
n^+ Thickness	5 μM
p^+ Surface Concentration	$10^{20}/cm^3$
n Doping Concentration	Variable
n^+ Doping Concentration	$10^{19}/cm^3$
Lifetime in p^+ Region	100 nsec
Lifetime in n Region	Iles data (1975)
Lifetime in p^+ Region	Iles date (1975)
Surface Recombination Velocity	10^3 cm/sec
Antireflecting Layer	"5 per cent Film"

The overall results regarding efficiency, open circuit voltage, and curve factor are summarized in Figure 4.3. Like the n^+-p-p^+ devices, these devices illustrate the same three regions of operation. The cutoff points for the regions however differ with respect to resistivity magnitude. High injection begins to occur above about 1 ohm-cm. The so called center region of operation is quite wide, extending to lower base resistivities. This is due mainly to the selction of equal hole and electron diffusion lengths from the data of Iles. Nonetheless it is seen that for base resistivities below 0.1 ohm-cm that there is a substantial decrease in efficiency due to the loss of collection efficiency.

4.3 Efficiency as a Function of Base Region Width

The p^+-n-n^+ devices were also investigated with regard to the effect of base region width upon the conversion efficiency. The devices are those of Table 4.1 except for the base resistivity, which was held constant at 0.3 ohm-cm. The surface region lifetime again was held at a constant 100 nsec in order to isolate the effect of the base region modification.

Figure 4.4 shows the results of these calculations. It can be seen that the efficiency remains relatively constant as the base width is decreased. These results are quite similar to those obtained with the n^+-p-p^+ devices which were discussed in detail in a prior section. It should be noted that back surface optical reflection is included in this analysis. If this is not included, the efficiency decreases more with decreasing width.

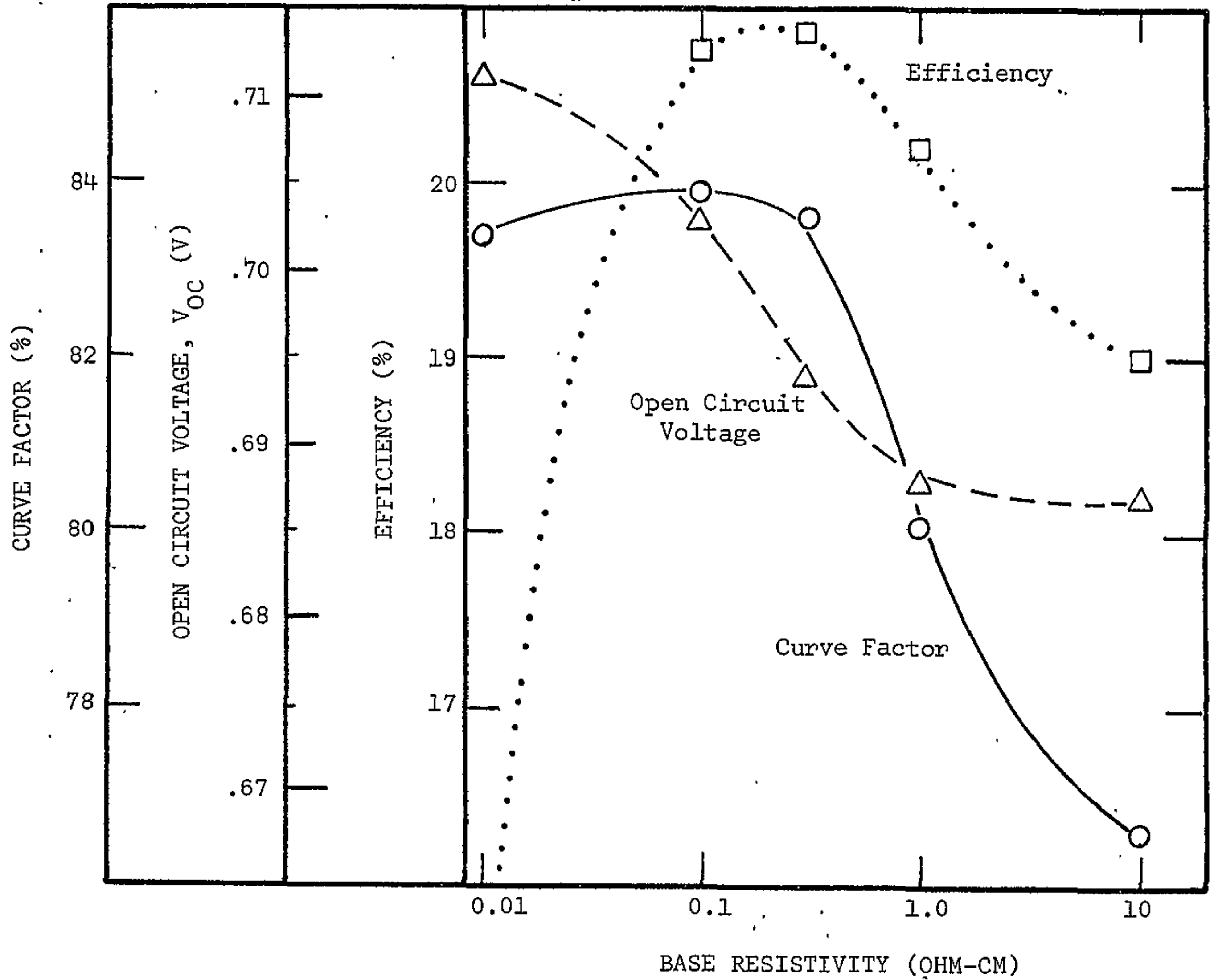

Figure 4.3 Summary of results for the p^+-n-n^+ solar cells (See Table 4.1)

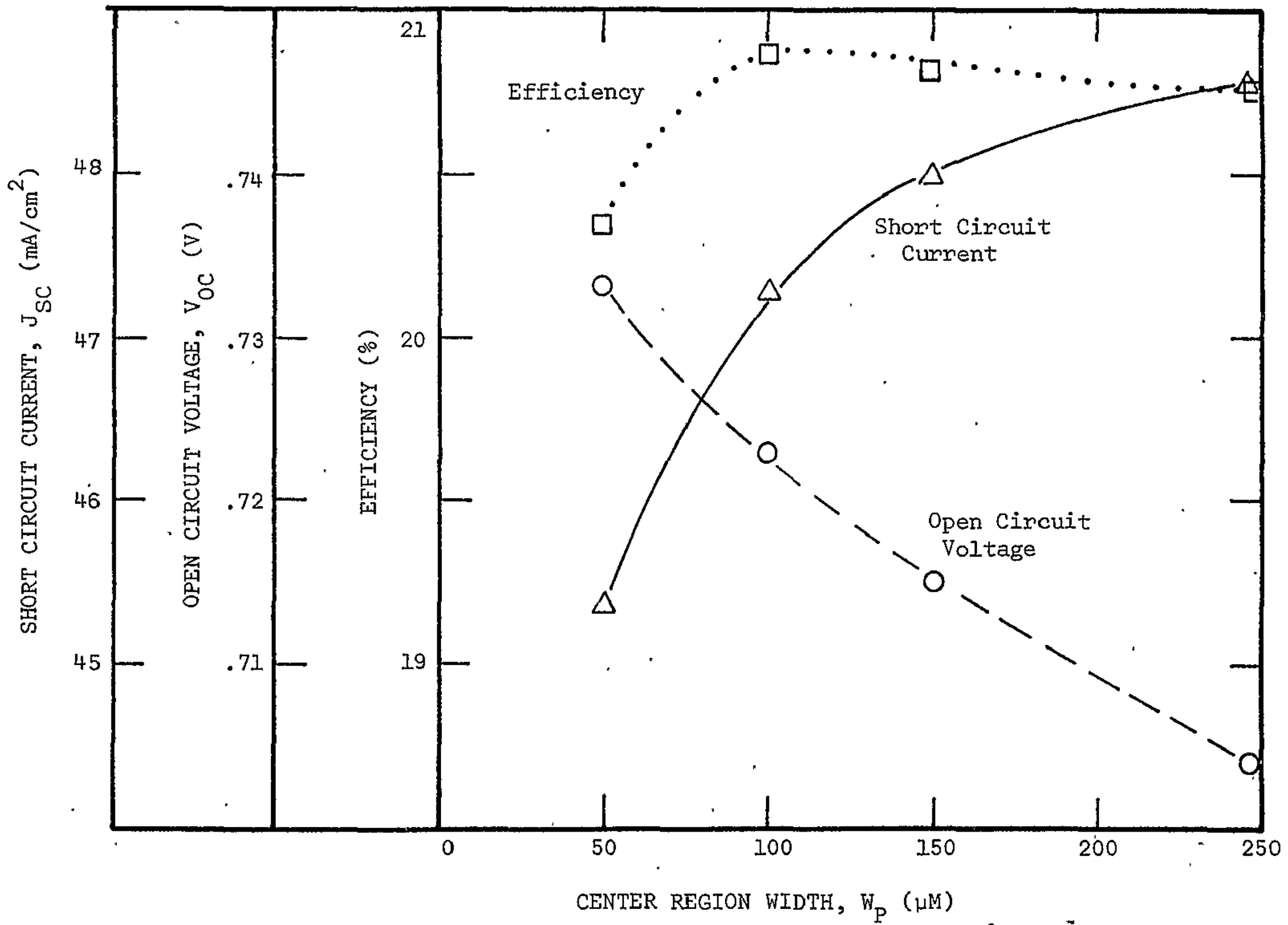

Figure 4.4 Results for the 0.3 ohm-cm p^+-n-n^+ solar cell as a function of center region width.

4.4 Lifetime Related Differences Between the n^+-p-p^+ and p^+-n-n^+ Structures

As stated in the prior sections, the electron and hole diffusion lengths were taken as identical in the calculations so far discussed. Due to differences in hole and electron mobility this produces larger lifetimes in the p type material. For this case the p^+-n-n^+ structure results in efficiencies which are higher than the n^+-p-p^+. This is mostly due to the increase in open circuit voltage due to the reduction of dark forward current injection. Recall that in a back surface field solar cell, the forward injection current (under dark conditions) is dependent upon the base region lifetime (assuming that the diffusion length in the base region is greater than the base width). However, if the hole diffusion length is taken as one-half of the electron diffusion length for the same doping level, the advantage of the p^+-n-n^+ structure disappears and the two structures are roughly equivalent. A slight difference does arise due to a reduction of short circuit current in the p^+-n-n^+ structure, but this is expected from the shorter diffusion length. The data tabulated in Table 4.2 illustrates these differences. These cells have the parameters presented in Table 2.1 with the appropriate changes in doping polarity. The base region doping is the same in both structures, $8.5 \times 10^{16}/cm^3$. This results in a 0.3 ohm-cm p-type base region and a 0.1 ohm-cm n-type base region. The major conclusion is that for similar cells with equal diffusion lengths, the p^+-n-n^+ cell has a slightly higher efficiency than the n^+-p-p^+ cell. However, if the hole diffusion length is reduced over that for electrons then the n^+-p-p^+ cell has the higher peak efficiency.

Table 4.2. Tabulation of Results Comparing the n^+-p-p^+ and p^+-n-n^+ solar cells.

	$\tau_{surface}$ nsec	τ_{base} (μsec)	V_{oc} (V)	CF %	Eff %	J_{sc} (mA/cm^2)	J_f at 0.7v (dark) (mA/cm^2)	Back Injection Component at 0.7v (dark) (mA/cm^2)
p^+-n-n^+	1	163	0.707	81.6	20.0	46.9	24.1	17
$L_p = L_n$ = 340 μM	100	163	0.718	84.6	21.1	46.9	38.2	3
p^+-n-n^+	1	41	0.679	81.8	18.9	46.1	91.4	33
$L_p = L_n/2$ = 170 μM	100	41	0.691	84.0	19.8	46.1	64.4	4
n^+-p-p^+	1	65	0.679	81.3	19.1	46.9	86.3	39
	100	65	0.692	84.1	20.2	47.0	63.8	17

The use of a smaller hole diffusion length is more consistent with existing experimental data on hole and electron lifetime and diffusion length.

5. THEORETICAL EFFECTS OF SURFACE DIFFUSED REGION LIFETIME MODELS ON SILICON SOLAR CELLS*

5.1 Introduction

This paper presents the results of a detailed computer simulation of narrow base silicon back surface field (BSF) solar cells. Such solar cells can be optimized with respect to open circuit voltage through reductions in the level of current injected into the base region. These theoretical optimizations however, produce open circuit voltages which are significantly higher than those found experimentally [1]. For the most part this discrepancy is due to the neglect or approximate modeling of the dark current component which is injected into the surface region. This current component can become quite significant and consequently can account for the lower values of open circuit voltage found experimentally. However, models which account for this current component can obtain a reasonable match with experimental results only by using extremely low (picosecond range) lifetimes in the surface region [2]. Such low lifetime values have been justified in past work on the basis that the surface region is a diffused region with a high level of trapping centers and dislocations. However, the present work has obtained a theoretical degradation in open circuit voltage without such extreme assumptions as to lifetime magnitudes. The work indicates that band gap shrinkage in the diffused surface layer combined with a spatially dependent lifetime form a mechanism for severe limitations on the open circuit voltage of solar cells formed by diffusion techniques.

*This chapter is written in the form of a paper which is being submitted for publication. References for this chapter are at the end of the chapter.

Certain spatial forms of lifetime dependence tend to shift the active area of the diffused region with respect to dark current density to a region very close to the surface. This, when combined with the fact that heavy doping effects are more severe near the surface, produces a pair of interacting mechanisms which greatly increases the current density injected into the surface region. The analytical method used in this work involves a numerical solution of the semiconductor device equations including the effects of a generation rate term due to AMO solar irradiance with a constant 5 per cent antireflection film and total optical reflection assumed at the back surface. The device modeling, which has been discussed elsewhere, includes phenomena such as drift and diffusion currents, recombination effects, doping dependent mobility, non-ohmic contacts, diffused impurity profiles, and band gap reduction due to heavy doping effects [3,4].

5.2 General Device Models

The basic solar cell structure studied is that of a n^{+}-p-p^{+} (or p^{+}-n-n^{+}) back surface field solar cell with the characteristics outlined in Table 5.1. Results by Michel et al. have been confirmed in that high efficiency solar cells can be fabricated with narrow base layer widths [5]. Subsequently a narrow (100 μM) base region is used in this work. The width of the base region, in combination with the low base resistivity, forms a situation in which carrier injection into the surface region tends to be the major component of the dark current density and subsequently in the determination of the open circuit voltage. Consequently the characterization of the diffused surface region is quite important. In particular, the characterization of the lifetime in this region is an important parameter and consequently

Table 5.1 Device parameters used in surface region study.

Parameter	Value
Diffused Surface Thickness	0.1 μM
Center Region Thickness	100 μM
Back Surface Region Thickness	5 μM
Surface Concentration (Gaussian)	$10^{20}/cm^2$
Center Region Resistivity	0.3 ohm-cm
Back Surface Region Concentration	$10^{19}/cm^2$
Surface Recombination Velocity	10^3 cm/sec
Antireflection Layer (Two Pass Model)	"5% Film"
Irradiance Conditions	AMO

is described in this work by two models. One is that of a constant lifetime, of either 1 nsec or 100 nsec, and the other is that of a spatial doping dependent model as postulated by Lindholm, *et al.* [6]. The general form of this doping dependent model is

$$\tau(x) = (\tau_o)/(N_S/N_B + 1)^N \tag{1}$$

where N_S is the doping in the diffused region, N_B is the bulk or base region doping, τ_o is a constant dependent upon the base or bulk region lifetime (τ_o equals τ_{no} for a p-type base layer and τ_{po} for a n-type base layer), and N is a parameter which can take on the values of 1, 2, or 4 [7].

The thin surface diffused region in solar cell structures is typically quite heavily doped. Consequently both Fermi-Dirac statistics and band gap reduction effects must be included in an analysis of this region. However, the magnitude of band gap reduction is a quantity not known with a great deal of certainty for silicon. The overall combined effect of degenerate doping and band gap reduction however is an increase in the intrinsic carrier concentration. This can be conveniently modeled by an "effective doping" which is the doping required to give the correct minority carrier density if Fermi-Dirac statistics and band gap reduction effects were not present. Figure 5.1 illustrates the effective doping in n-type material for several band gap reduction models including the empirical model used in this work [8,9,10,11,12]. The curves for Mock and van Overstraeten were obtained directly from their results regarding an effective intrinsic concentration. The other curves were calculated from reported models for band gap shrinkage. These models were used with Fermi-Dirac statistics to determine the effective doping. In addition,

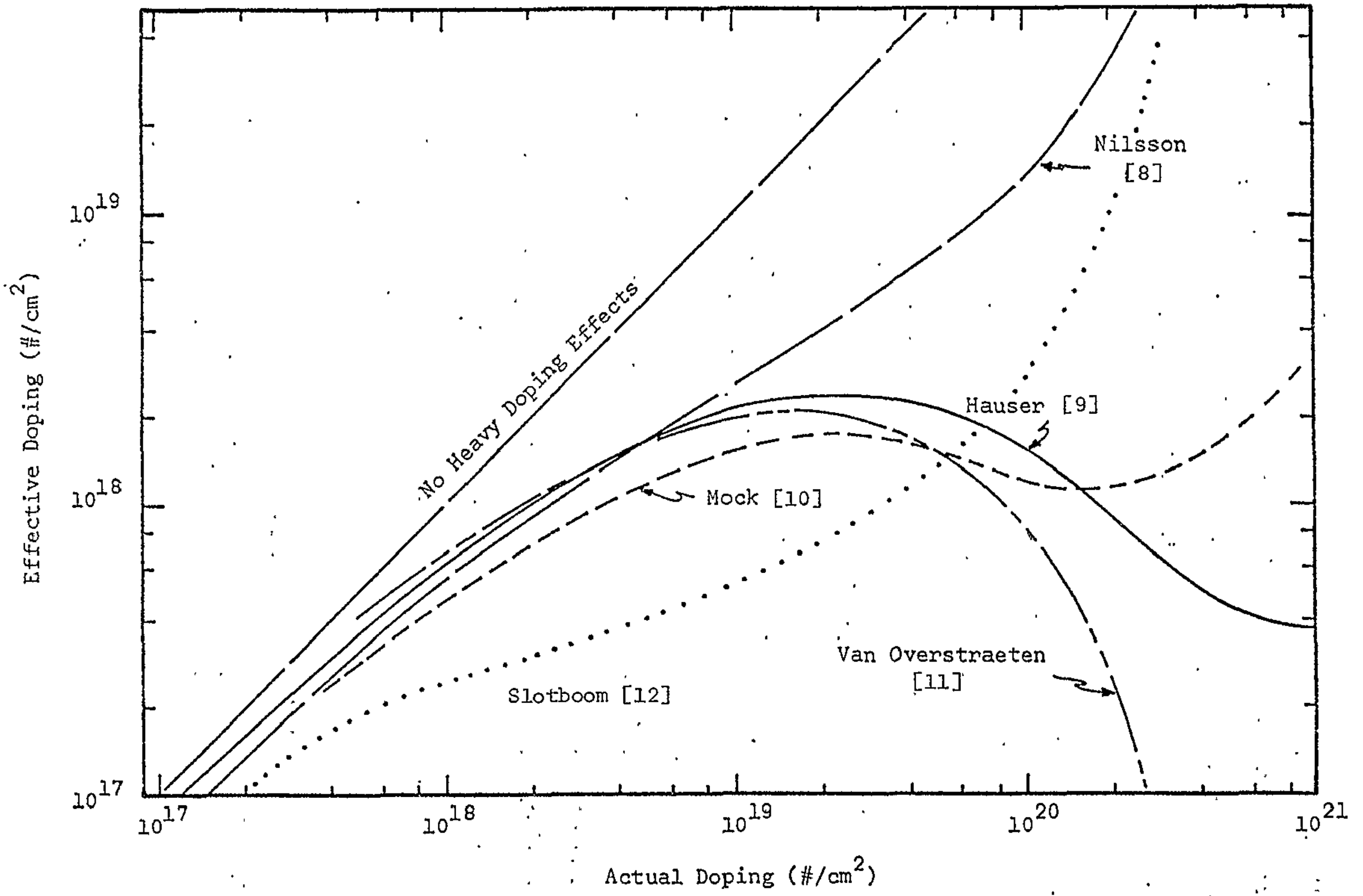

Figure 5.1 Various models illustrating the effective doping arising from heavy doping effects.

the effective doping differs for n-and p-type material due to a difference in the Fermi level penetration into the conduction and valence bands. This is illustrated in Figure 5.2. Note also in this figure curves for the effect of Fermi-Dirac statistics independent of any band gap reduction. The band gap reduction effects tend to form a peak in the effective doping for n-type material at an actual doping density of about $2x10^{19}/cm^3$ and an effective doping density at about $2x10^{18}/cm^3$. This peak suggests an optimum doping density around $2x10^{19}/cm^3$ for minimizing heavy doping effects but the exact doping density at which this occurs depends on the model used for band gap reduction.

5.3 Results

The heavy doping effect in itself tends to increase the injected current density into the surface region due to an increase in minority carrier density. However, the increase is much more severe than expected when spatial lifetime effects are also included. It can be shown from first order device theory neglecting heavy doping effects (confirmed by the complete analysis) that in the diffused surface layer, under dark conditions

$$p(x) \simeq \frac{n_i^2}{N_s(x)} \exp(qV/kT), \qquad (2)$$

where p is the minority carrier density and N_s is the doping density. The change in current density in the diffused region can be expressed as

$$\Delta J(x) = \int_0^x Q(x)/\tau(x)dx, \qquad (3)$$

where Q is the charge in the region, τ is the lifetime in that region, and x = 0 is taken as the depletion region edge. Combining Equations (1) and (2), it can be seen that (also assuming that $N_s >> N_B$)

REPRODUCIBILITY OF THE ORIGINAL PAGE IS POOR

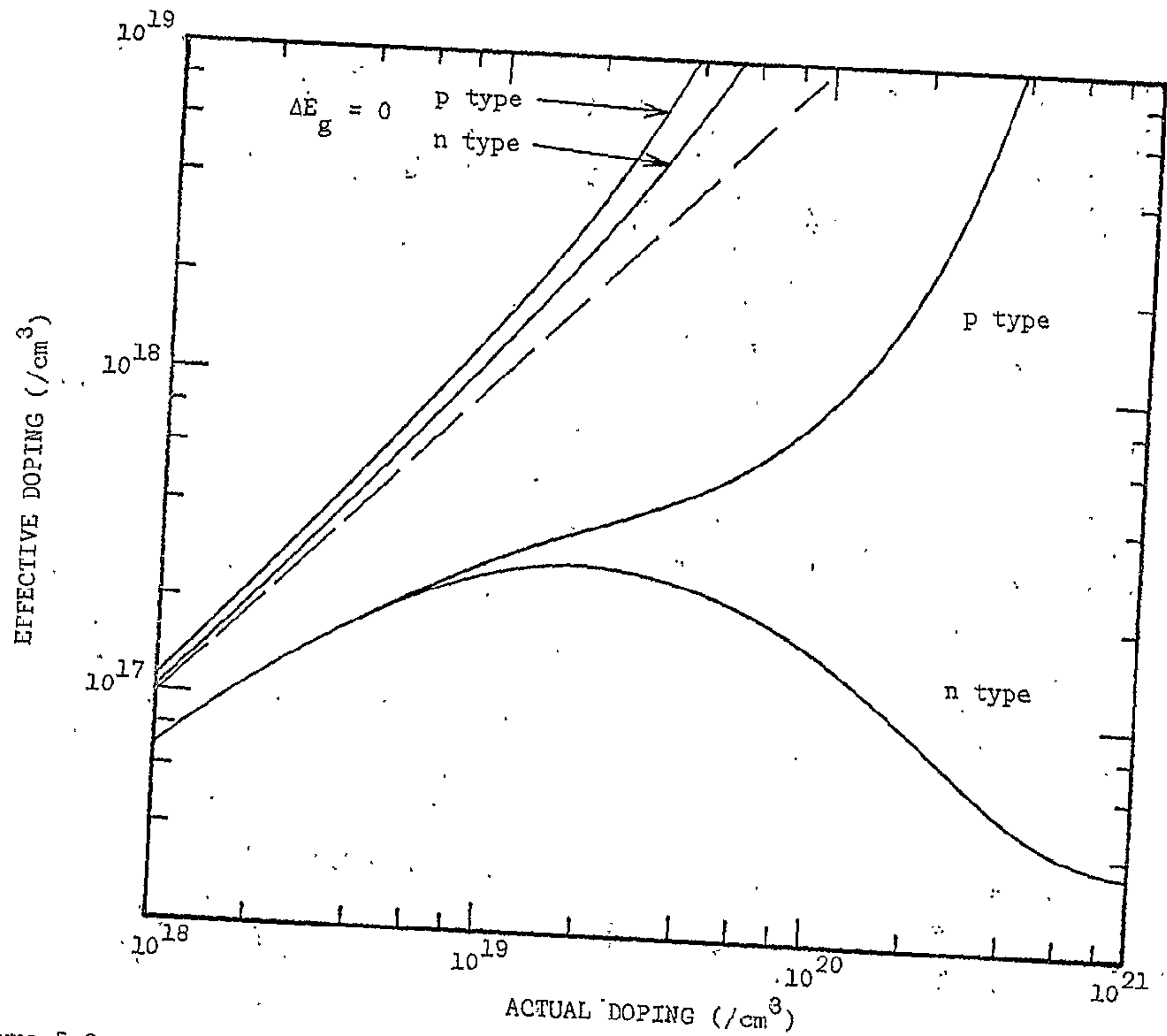

Figure 5.2 Variation of effective doping for different types of doping utilizing an empirical bandgap reduction model [9].

$$Q/\tau \; \alpha \; N_s^{N-1}. \qquad (4)$$

Consequently for values of N greater than 1 the integrand in Equation (3) tends to grow in magnitude for increasing x. This is in contrast to the idea that the region close to the injecting junction is the most important in determining injection current density. Consequently heavy doping effects, which are larger closer to the surface, have a stronger effect for these cases. If heavy doping is included in the model,

$$Q/\tau \; \alpha \; N_s^{N}/N_{eff} \qquad (5)$$

since the lifetime is dependent upon the actual doping (N_s) and the minority carrier density is dependent upon the effective doping (N_{eff}).

Plots of Q/τ as obtained from the computer analysis are shown in Figure 5.3 throughout the diffused surface layer. The doping profile in the surface layer has been taken to be described by a Gaussian function of distance. The dashed curves in Figure 5.3 indicate the variance of Q/τ for no heavy doping effects and different N values. For the N = 0 case (i.e. constant lifetime) the decay in Q/τ with increasing distance from the depletion region is as expected for the given doping profile. However the N=1 case indicates that the entire surface region contributes about equally to current flow. (The lowered values of Q/τ are indicative of the higher lifetime which occurs for the N = 1 case). The N = 2 case however indicates that the region close to the surface produces significantly more recombination current than regions close to the injecting junction. The calculated behavior is seen to follow almost exactly the simple results of Equation (4).

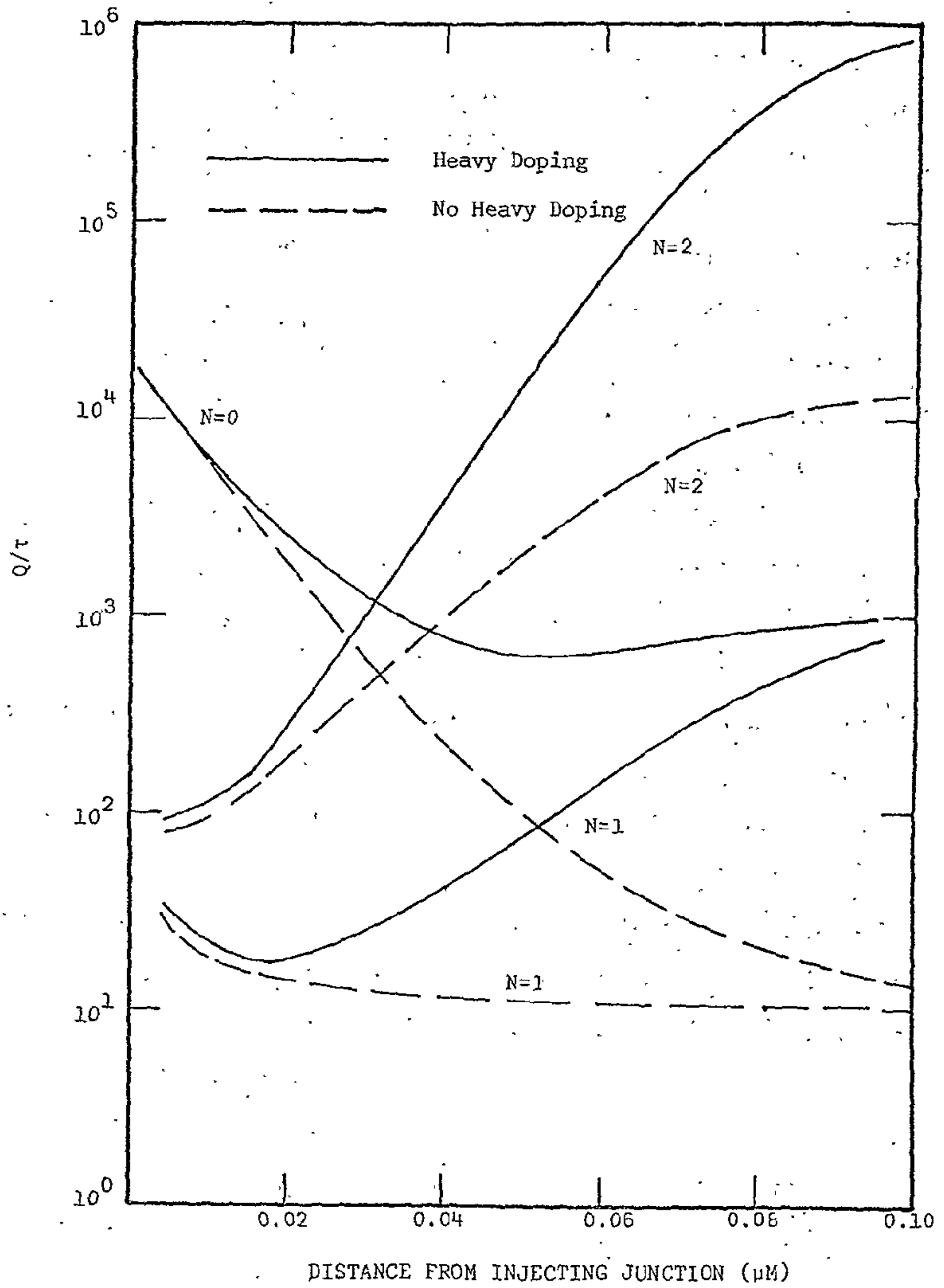

Figure 5.3 The dependence of the quantity Q/T for various values of the spatial lifetime parameter, N.

The solid curves indicate the situation when heavy doping is included. Here there is an enhanced significance of the surface region in all cases due to the reduction in the effective doping near the surface. For the case of constant surface region lifetime (N=0) the heavy doping effect is present although its contribution is not as significant as in the other cases as seen from the high value of Q/τ near the injecting junction. For N>0, the lifetime near the injecting junction is sufficiently high to shift the active region further toward the semiconductor surface.

Figure 5.4 indicates the effect of this recombination upon the buildup of current in the diffused region. This figure neglects the current component due to surface recombination for the sake of clarity. The importance of the diffused layer close to the surface is seen to be enhanced in importance when heavy doping and a spatial decay in lifetime is taken into account. For the N = 1 and N = 2 cases it is seen that about 80% of the dark current component due to the surface region comes from about 20% of the diffused layer located near the semicondcutor surface.

Table 5.2 summarizes the effects of these heavy doping and lifetime effects on solar cell terminal characteristics. The surface region current component is the current component injected into the n^+ (n^+-p-p^+ cell) or p^+ (p^+-n-n^+ cell) region. It is this injection component which is responsible for reductions in open circuit voltage and efficiency in low resistivity solar cells. This component includes both the depletion region and surface recombination components. For the lifetime models used, the depletion region current component was found to be insignificant except for the constant (1 nsec) model. The first two rows of Table 5.2 indicate the extent of the heavy doping effect upon the surface region current.

REPRODUCIBILITY OF THE
ORIGINAL PAGE IS POOR

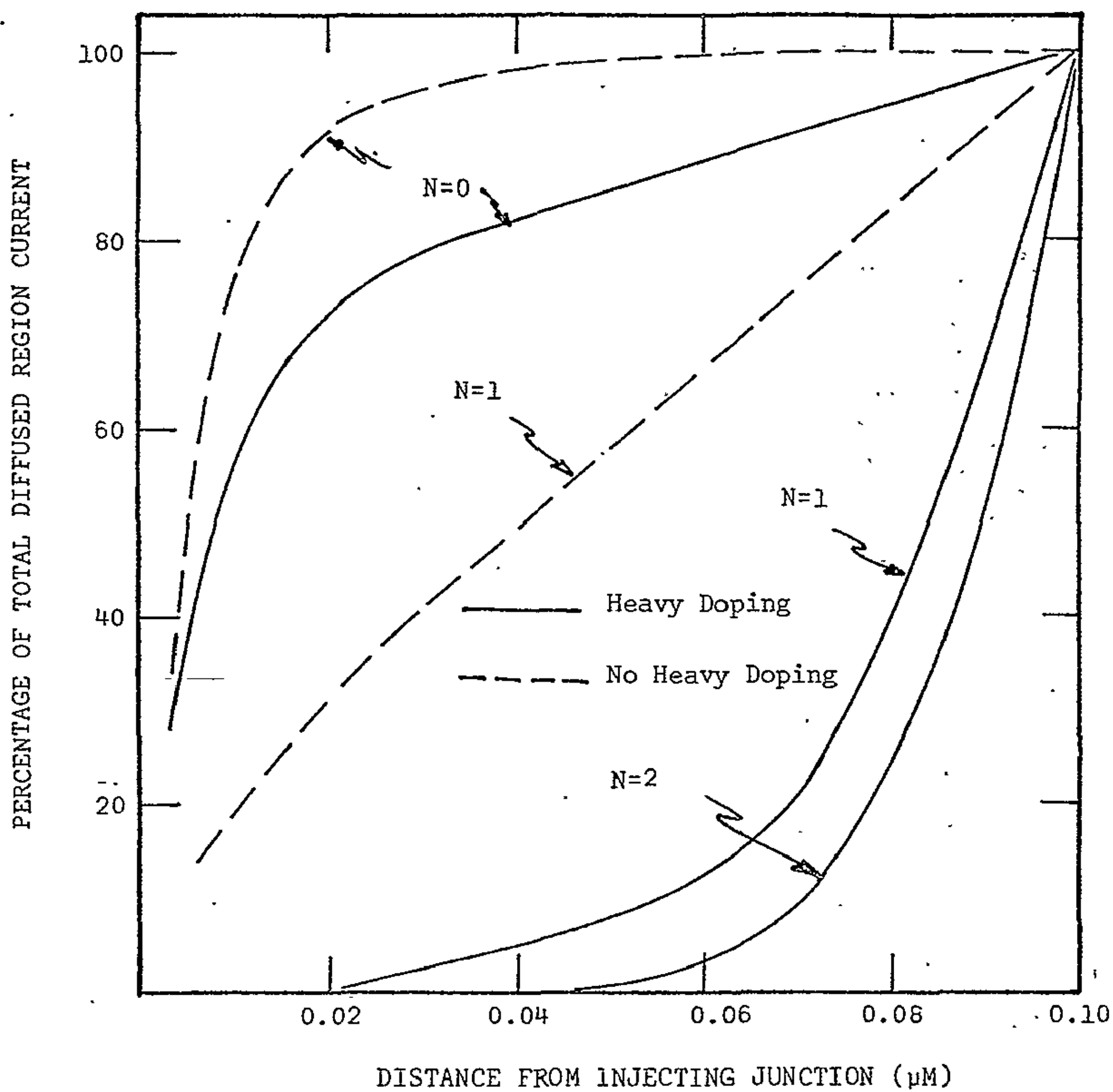

Figure 5.4 Buildup of diffused region current as a function of the spatial lifetime parameter, N.

Table 5.2 Summary of terminal characteristics

Structure	Heavy Doping Effects	Diffusion Length Ratio (L_n/L_p)	Efficiency (%)	Open Circuit Voltage (Volts)	Short Circuit Current (mA/cm^2)	Total Current @ 0.7v Dark (mA/cm^2)	Surface Region Current Component @ 0.7v Dark (mA/cm^2)
n^+-p-p^+ (Constant 1 nsec n^+ region life-time)	No	1	20.0	0.70	46.9	53	12
	Yes	1	19.1	0.68	46.9	86	39
n^+-p-p^+ (N = 2)	No	1	20.3	0.70	46.9	46	5.3
	Yes	1	18.8	0.65	46.6	270	230
	Yes	2	17.6	0.63	45.8	730	680
p^+-n-n^+ (N = 2)	No	1	20.8	0.71	46.7	31	19
	Yes	1	19.3	0.67	46.7	150	130
	Yes	2	18.8	0.66	45.8	190	130
n^+-p-p^+ (N_s = $2x10^{19}/cm^3$, N = 2)	No	1	20.5	0.70	47.0	43	2.3
	Yes	1	20.2	0.69	47.0	63	17

The increase in surface injection from 12 mA/cm^2 to 39 mA/cm^2 when heavy doping is included causes about a 3 percent decrease in the open circuit voltage for this constant lifetime case. However, the equivalent structure with a spatially dependent lifetime (N = 2) illustrates a very large increase (a factor of 43) in surface region current when heavy doping is included. For this case these two effects have combined to cause a 7 per cent decrease in the open circuit voltage. Comparing these results to the first two rows of the p^+-n-n^+ cell it can be seen that the heavy doping effects are less significant in p^+-n-n^+ cells than in n^+-p-p^+ cells as expected. However, all these results are quite lifetime dependent. For example, if the assumption is made that the hole diffusion length is half the electron diffusion length (where the electron diffusion length for the bulk material is taken from the data of Iles) then more severe results are obtained as seen from the table. It can also be concluded that greater band gap reductions than those used in the present work will also tend to increase the severity of these heavy doping effects. However, the severity of the effect is not as great as one might expect. For example, a 10 per cent increase in the amount of band gap reduction resulted in an increase of injection current density by a factor of about 1.5. The recent data on band gap reduction by Slotboom and Graaf [12] resulted in a reduction of this same current component by a factor of 0.7. This can be expected from their data since it indicates less of a band gap shrinkage at higher doping but more shrinkage at lower doping than the present model. (See Figure 5.1).

Godlewski [13] found that an optimum surface doping level could be established which removes any retrograde fields in the n^+ surface region

due to heavy doping effects. That work was based on a uniform diffused region lifetime and the pessimistic model for band gap reduction presented by Van Overstraeten [11]. The last entry in Table 2 indicates the present computer results for a cell with an optimum surface concentration. Indeed, less of a dependence on heavy doping effects can be seen. However, this is likely caused in the present study by a combined increase in diffused region lifetime as well as the overall reduction in band gap shrinkage. Both of these effects tend to hold the open circuit voltage at a higher level, contributing to the effects of removing the retrograde field. In addition, it is significant that the removal of the retrograde field did not produce any significant change in the short circuit current density. Spectral response calculations have further indicated that the combined effects of a spatially dependent lifetime and heavy doping effects do reduce the short wavelength response to values about 25% below that of the constant lifetime case with heavy doping. The amount of reduction however is dependent upon the surface recombination velocity and the band gap reduction model utilized.

5.4 Summary

It has been found that band gap reduction and a spatial decay in lifetime can combine to produce significant effects upon the spatial nature and magnitude of the injection current density into the diffused surface region of solar cells. The spatial nature of the injection current is primarily dependent upon the rate of decay of the lifetime with impurity concentration. The magnitude of this current component is dependent upon both the magnitude of the lifetime parameter and the amount of band gap shrinkage in the region. In all cases except for that of a constant lifetime it has been found that regions away from the injecting junction and close to the surface play a far

more important role in carrier injection than previously expected. These effects differ for n-and p-type surface regions with the p-type surface region producing smaller components of back injected current. These conclusions depend somewhat upon the lifetime values selected and these effects can be reduced through the selection of a lowered impurity concentration at the semiconductor surface. This both reduces the band gap reduction and increases the lifetime in that region at the cost of an increase in sheet resistivity of the surface layer. Overall it can be concluded that the diffused surface region can reduce the open circuit voltage as experimentally observed due to the combined effects of heavy doping and a spatial dependence of lifetime. Furthermore, spectral response calculation indicate that these same mechanisms can combine to reduce the short wavelength response. These results indicate that very careful attention must be given in solar cell fabrication to minority carrier lifetime in the diffused surface layer very near the solar cell surface if the ultimate potential of silicon solar cells is to be realized.

REFERENCES

1. H. W. Brandhorst, International Electron Devices Meeting, 331 (1975).

2. J. G. Fossum, International Electron Devices Meeting, 339 (1975).

3. P. M. Dunbar and J. R. Hauser, 11th Photovoltaic Spec. Conf. 13 (1975).

4. P. M. Dunbar and J. R. Hauser, Solid State Electronics, 19, 95 (1976).

5. J. Michel, A. Mircea, and E. Fabre, Journal of Applied Physics, 46, 11, 5043 (1975).

6. F. A. Lindholm, S. S. Li, and C. T. Sah, 11th Photovoltaic Spec. Conf. 3 (1975).

7. P. A. Iles and S. I. Soclof, 11th Photovoltaic Spec. Conf. 19 (1975).

8. N. G. Nilsson and K. G. Svantesson, Solid State Communications, 11, 155 (1972).

9. J. R. Hauser, Final Report on NSF Grant GK-1615 (1969).

10. M. S. Mock, Solid State Electronics, 16, 1251 (1973).

11. R. J. Van Overstraeton, et al., IEEE Trans. Electron. Dev. ED-20, 290 (1973).

12. J. W. Slotboom and H. C. de Graaff, International Electron Devices Meeting Supplement, 14 (1975).

13. M. P. Godlewski, et al., 11th Photovoltaic Spec. Conf. 32 (1975).

6. SPECIAL DEVICE STUDIES

6.1 Epitaxial Structures

Epitaxial silicon solar cell structures of late have attracted some interest due to the ability to take advantage of equilibrium field effects made possible by tailored doping profiles. Two such structures have been analyzed. The first of these is a p^+-p-n-n^+ device presented by R. V. D'Aiello *et al.* which includes a graded base region as well as a high-low junction. The second structure is somewhat similar except for geometric changes in order to further enhance the efficiency.

The doping profile of the D'Aiello structure is a relatively narrow device, with a 15 μM wide back region high-low junction and a graded base region. The overall device is 50 μM in width, with a 1 μM wide diffused surface region. The base grading varies exponentially from $10^{18}/cm^3$ to $10^{16}/cm^3$. The surface region is p-type, with a region of uniform doping along with that of a Gaussian diffusion. In analyzing this structure, the lifetime data of Iles was used throughout the base and high-low junction region. However, two models were used within the surface region. The first of these was that of a constant lifetime (1 nsec) and the other utilized the spatial form described in the previous chapter (N=2). No heavy doping effects were included in the surface region.

The resulting dark characteristics are indicated in Figure 6.1. The large difference in these results is due to the surface region lifetime model. The dashed curve is for the constant lifetime case (1 nsec) whereas the solid curve is for the case where the lifetime is spatially dependent. In the latter case injection into the surface region amounts to only about 2 per cent of the total dark current density whereas this component is the predominant component in the constant lifetime situation. The constant

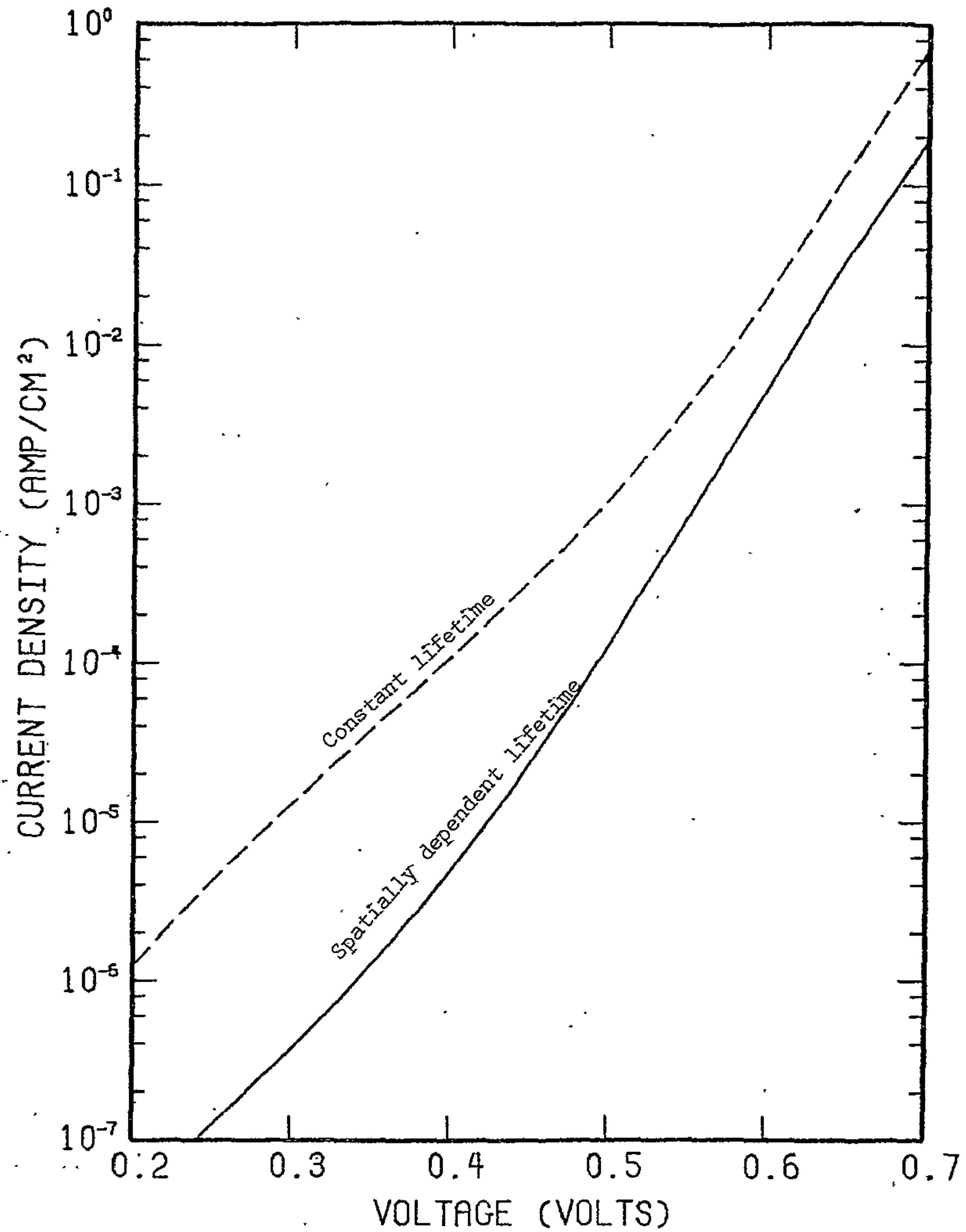

Figure 6.1 Dark characteristics of the D'Aiello structure.

low lifetime assumption is probably not appropriate for this structure due to the uniformly doped segment of the surface region. Figure 6.2 indicates the calculated electrostatic potential within the base region. Figure 6.3 and 6.4 indicates the electron and hole carrier densities within both the base and surface regions for various applied voltages. Due to the light doping at the junction interface it can be seen from these figures that a region of high injection is beginning to occur at around 0.7 v.

The illuminated characteristics for these structures are indicated in Figure 6.5. Again, the surface region lifetime has an appreciable effect upon both the open circuit voltage and the short circuit current. The effect of low lifetime on short circuit current is large due to the rather wide (1 μM) surface region width. In both cases however, the short circuit current density is low as compared to the available optical current for a device with an 800 Å SiO antireflection layer, which is in a range from 40 to about 45 mA/cm^2. There are several reasons for this. Most importantly, the device is quite narrow for optimum collection and in addition there is no reflection at the back contact. Secondly, the highly doped n^+ region is quite wide, being of the order of 15 μM. With this high a doping, collection efficiency is degraded due to recombination in the region. This is illustrated in Figure 6.6 which indicates the absolute value of the minority carrier density under short circuit conditions. The point at which the current density changes sign indicates the maximum depth of carrier collection which is just over 40 μM. It is clear the carriers generated in the back surface n^+ region are lost due to recombination. The lifetime in such a low resistivity region is approximately 35 nsec. Figure 6.7 indicates the carrier density distribution throughout the device. The effect of the built in potential

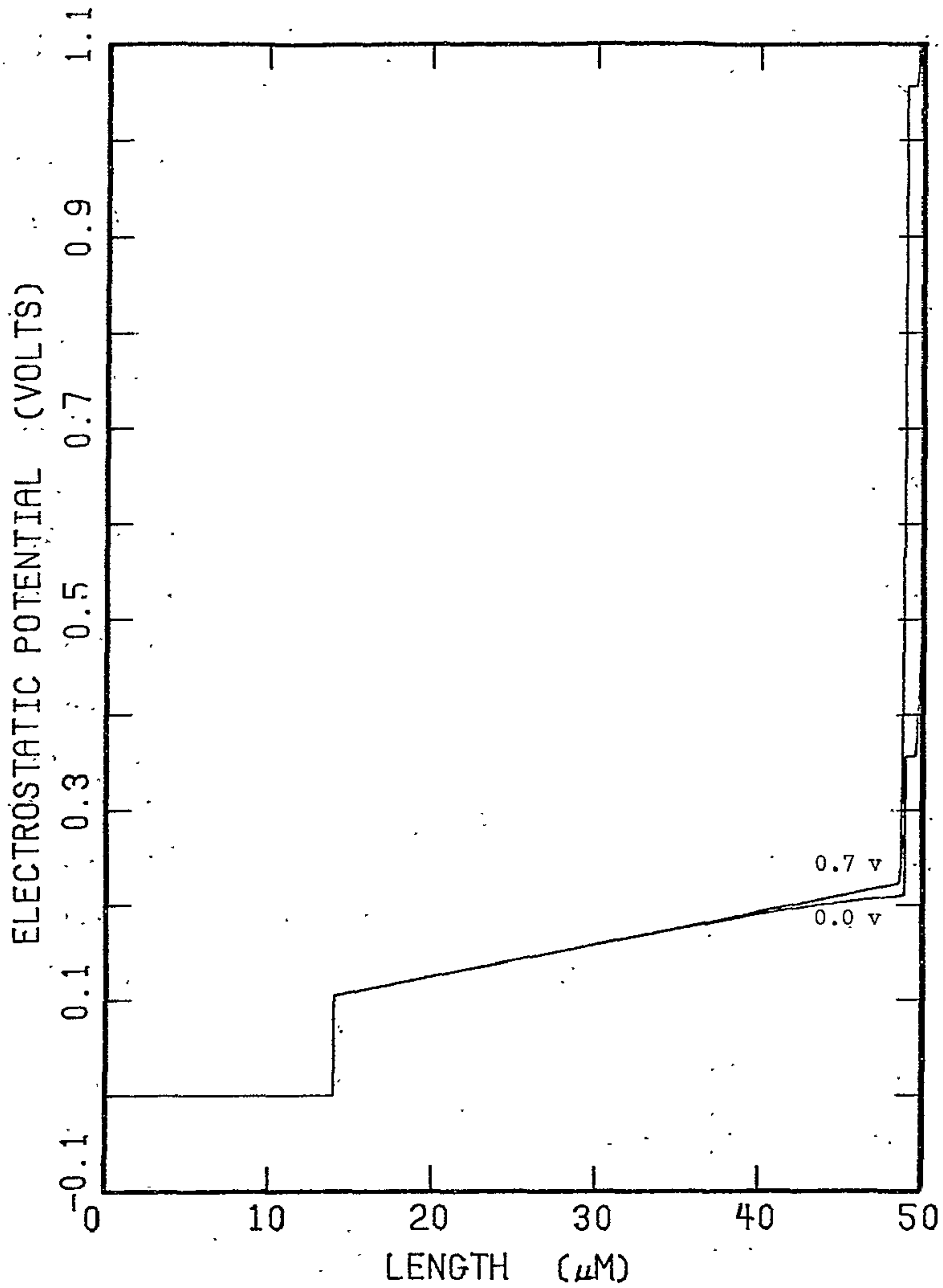

Figure 6.2 Electrostatic potential distribution over the entire D'Aiello device.

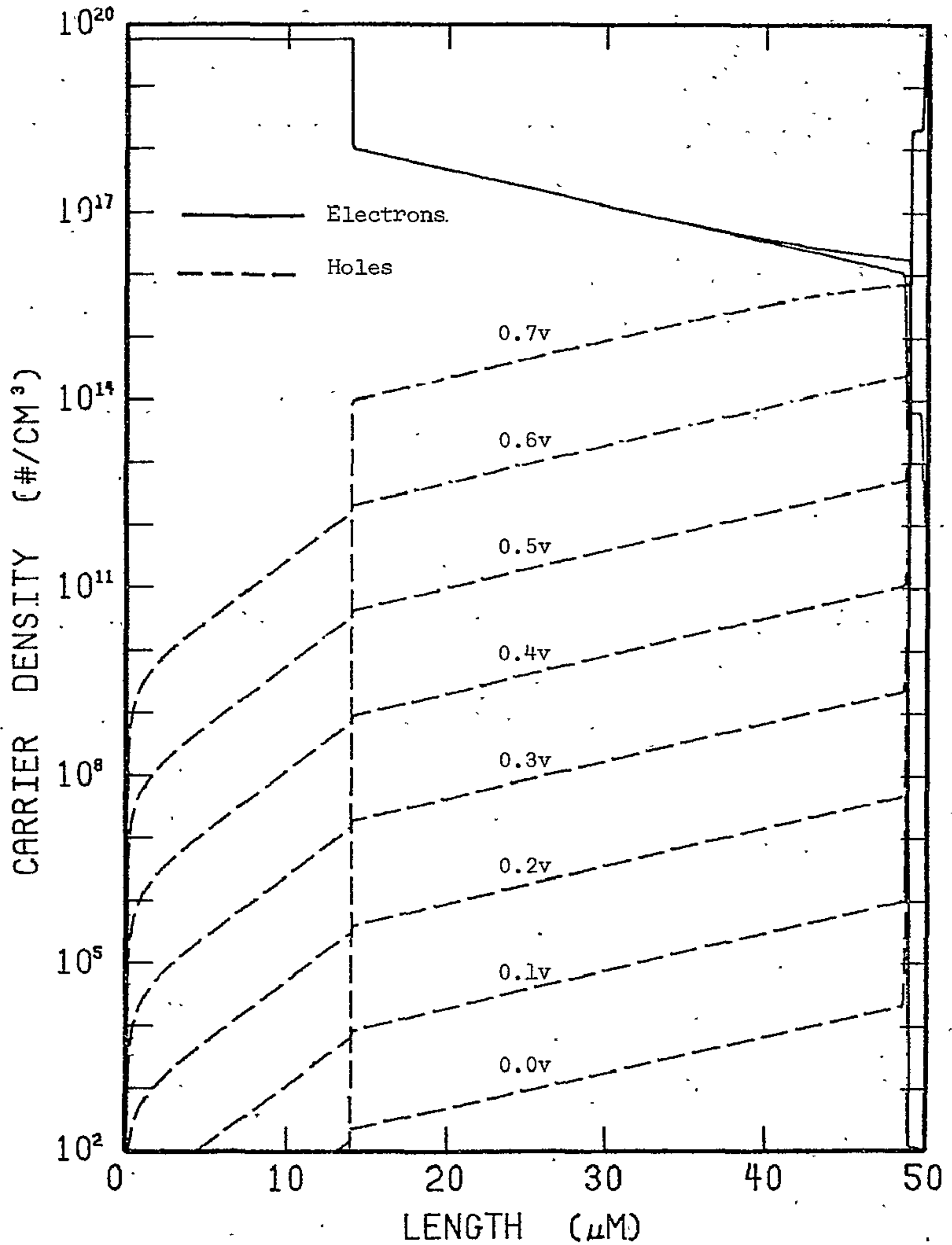

Figure 6.3 Dark carrier density distribution over the entire device for various applied voltages.

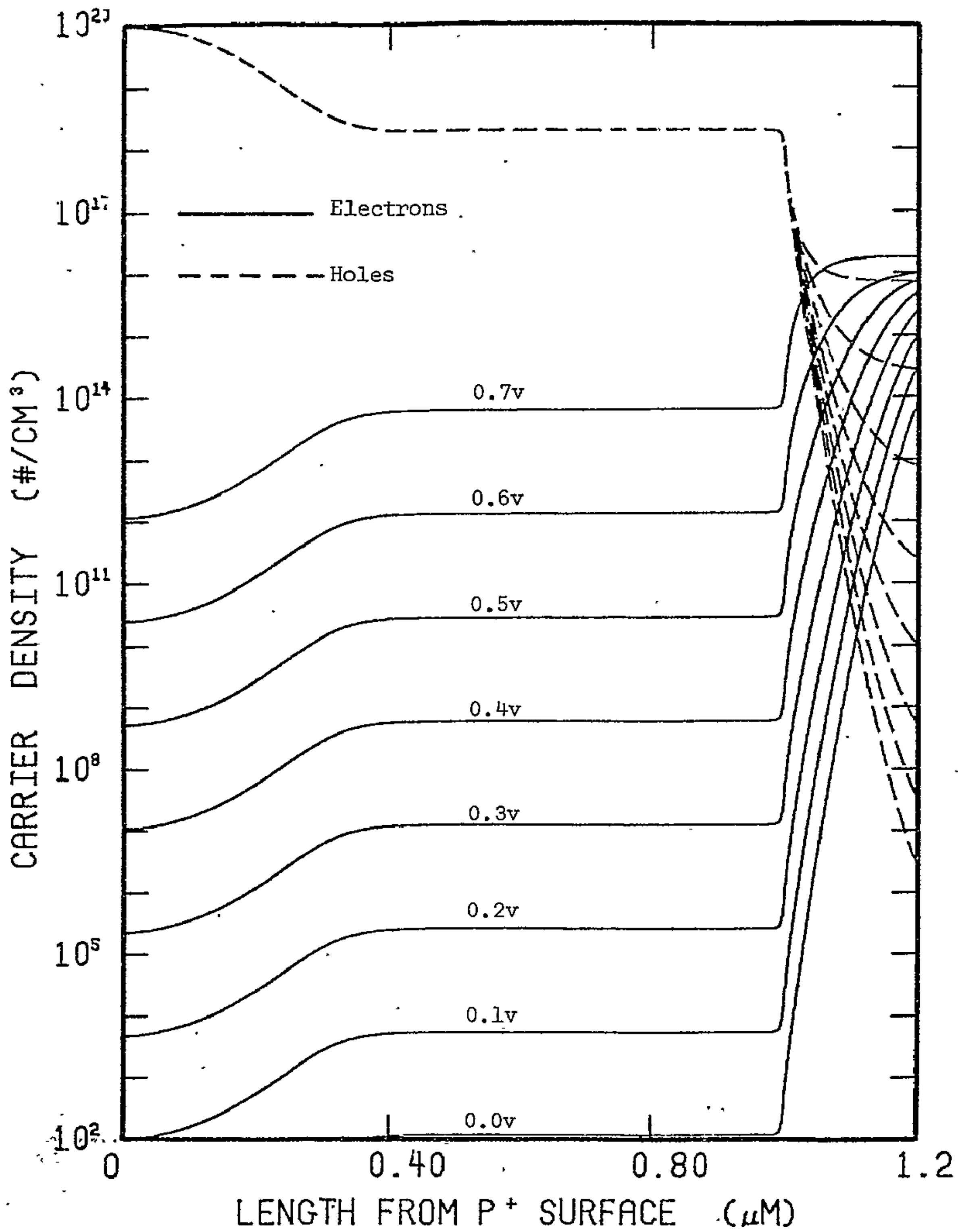

Figure 6.4 Dark carrier distribution in the surface region of the D'Aiello structure for various applied voltages.

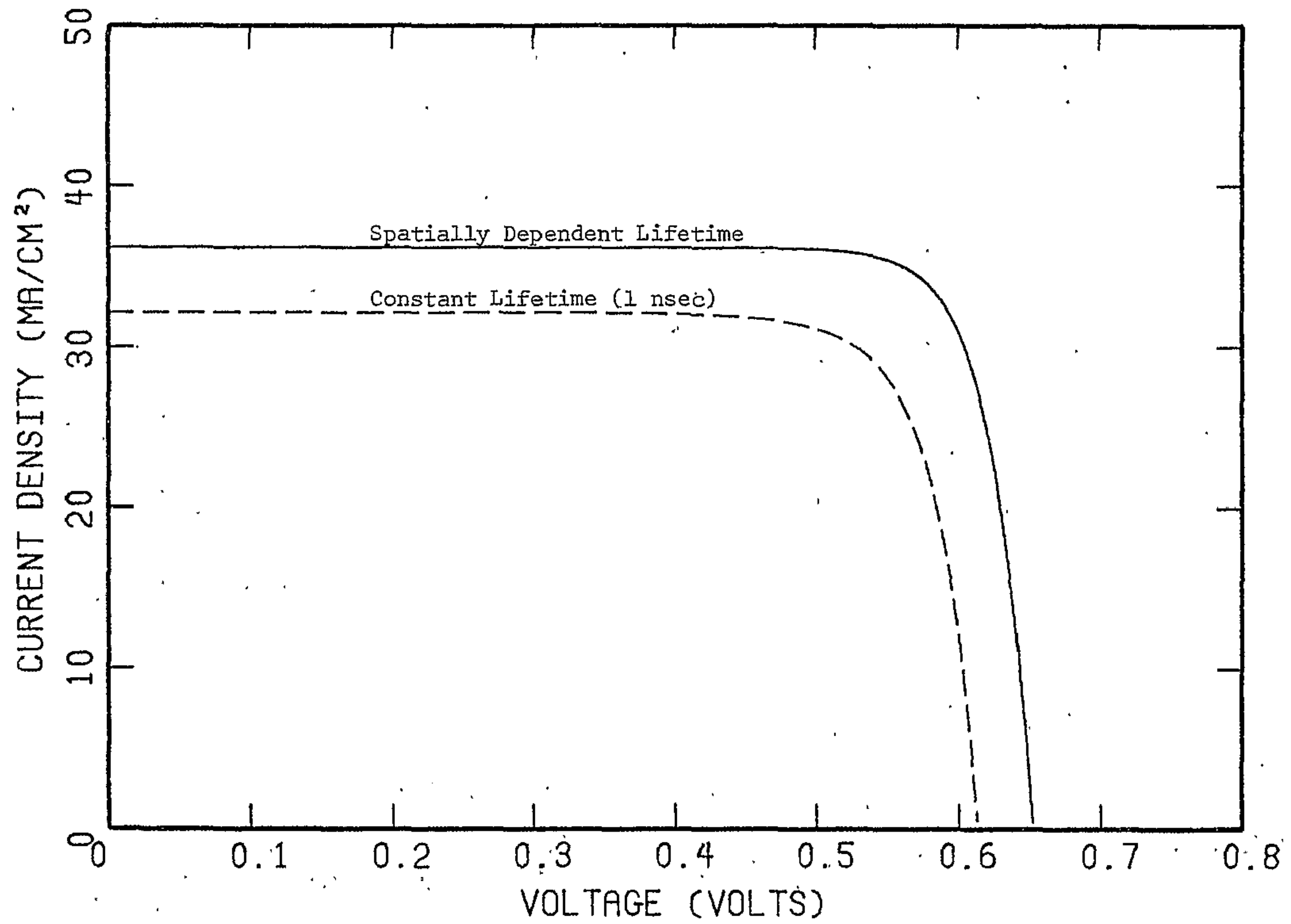

Figure 6.5 Illuminated J-V characteristics for the D'Aiello structure (AMO).

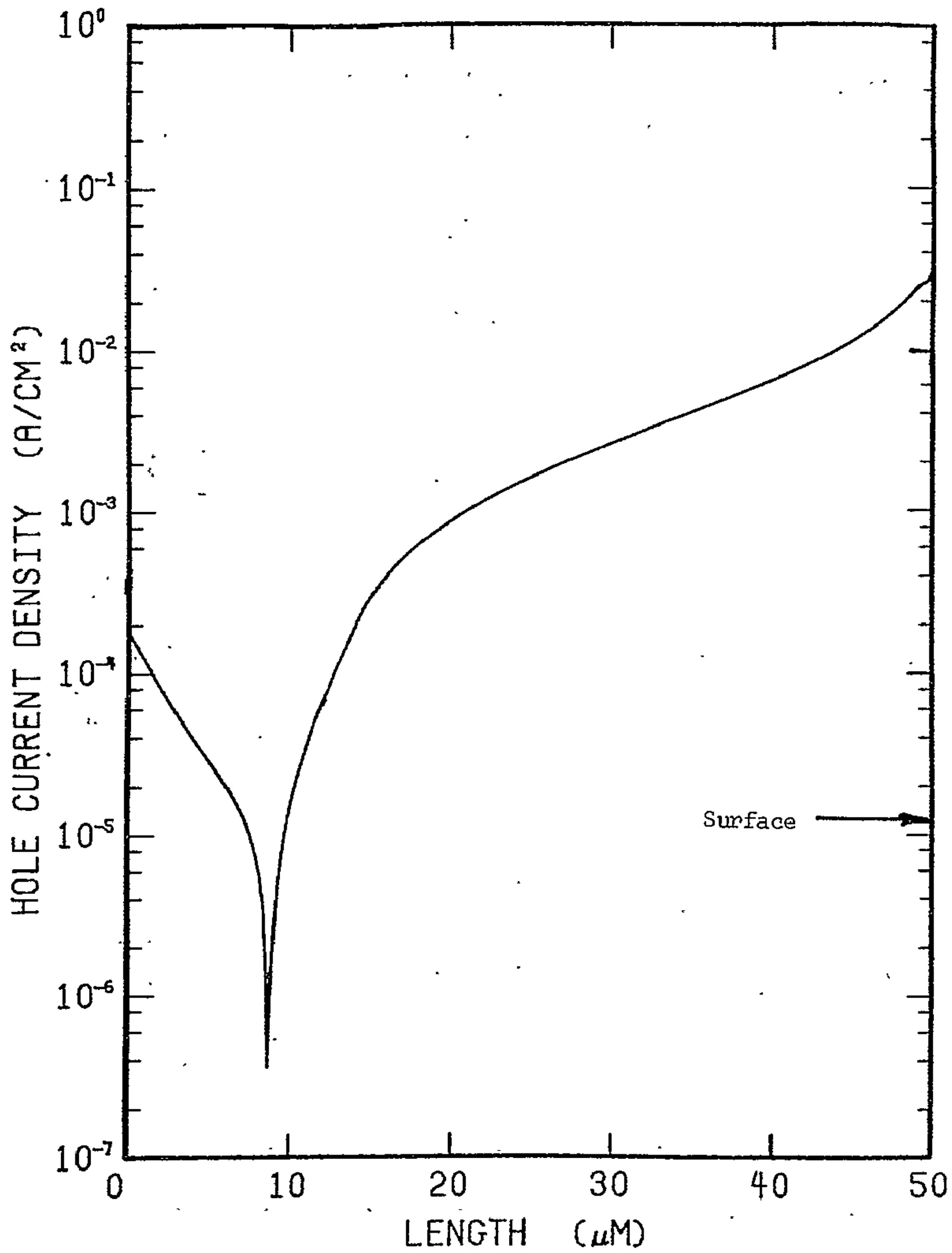

Figure 6.6 Hole current distributions for the D'Aiello structure for short circuit condition (AM0).

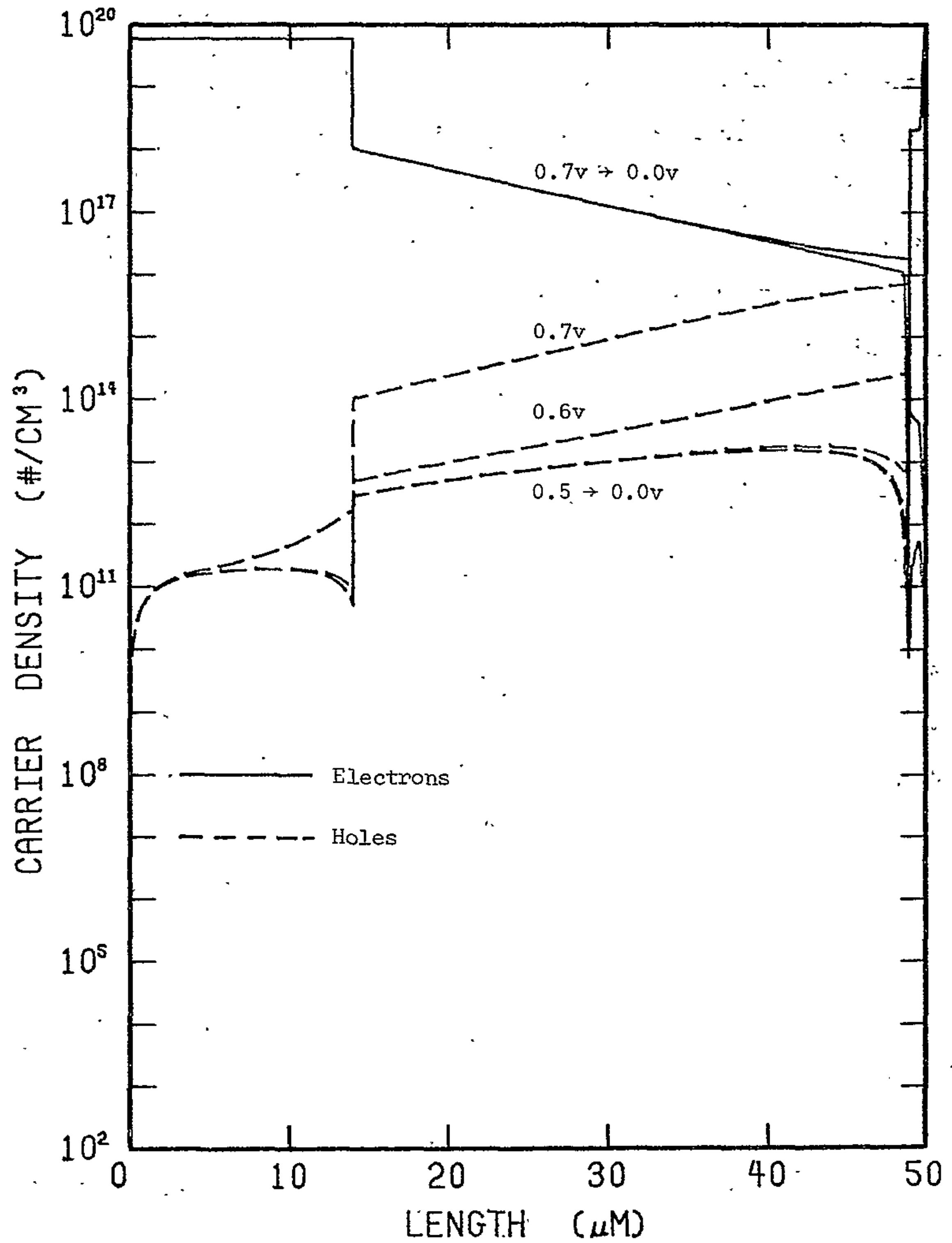

Figure 6.7 Carrier distribution over the entire device for various applied voltages (AMO illumination).

within the base region is apparent in the nonuniform carrier density due to the field pulling the carriers toward the collecting junction. With regard to the surface region, the advantage of having a region of uniform doping is not readily apparent. For the low lifetime case there is no advantage. For the spatial lifetime model, the results which follow indicate that there is little difference between this profile and one which simply has a thin diffused region. Figure 6.8 indicates the carrier distribution in the surface region for illuminated conditions.

The values of open circuit voltage and short circuit current calculated compared quite well with the measured data for the case where the spatial lifetime model is included. D'Aiello's data indicates an open circuit voltage of 0.64 v and short current density of about 34 mA/cm^2. The calculated open circuit voltage was 0.65 V with a short circuit current density of 36 mA/cm^2 with a peak efficiency of 14.5 per cent. The inclusion of heavy doping effects would have lowered the calculated open circuit voltage somewhat, but the effect would not be great since the amount of surface injection is not a large fraction of the total current density. In addition, heavy doping effects in a p-type region are not as severe as in a n-type region.

The second epitaxial type structure analyzed is a modification of the prior structure. However it still inclues a high-low junction as well as a graded base region. The profile selected for this device is shown in Figure 6.9. The four base region profiles indicate additional variation in the nature of the graded base region as represented by the 0.3, 1, 10, and 100 ohm-cm base resistivity at the junction. The overall device is much wider than the prior structure in order to collect more of the available

REPRODUCIBILITY OF THE
ORIGINAL PAGE IS POOR

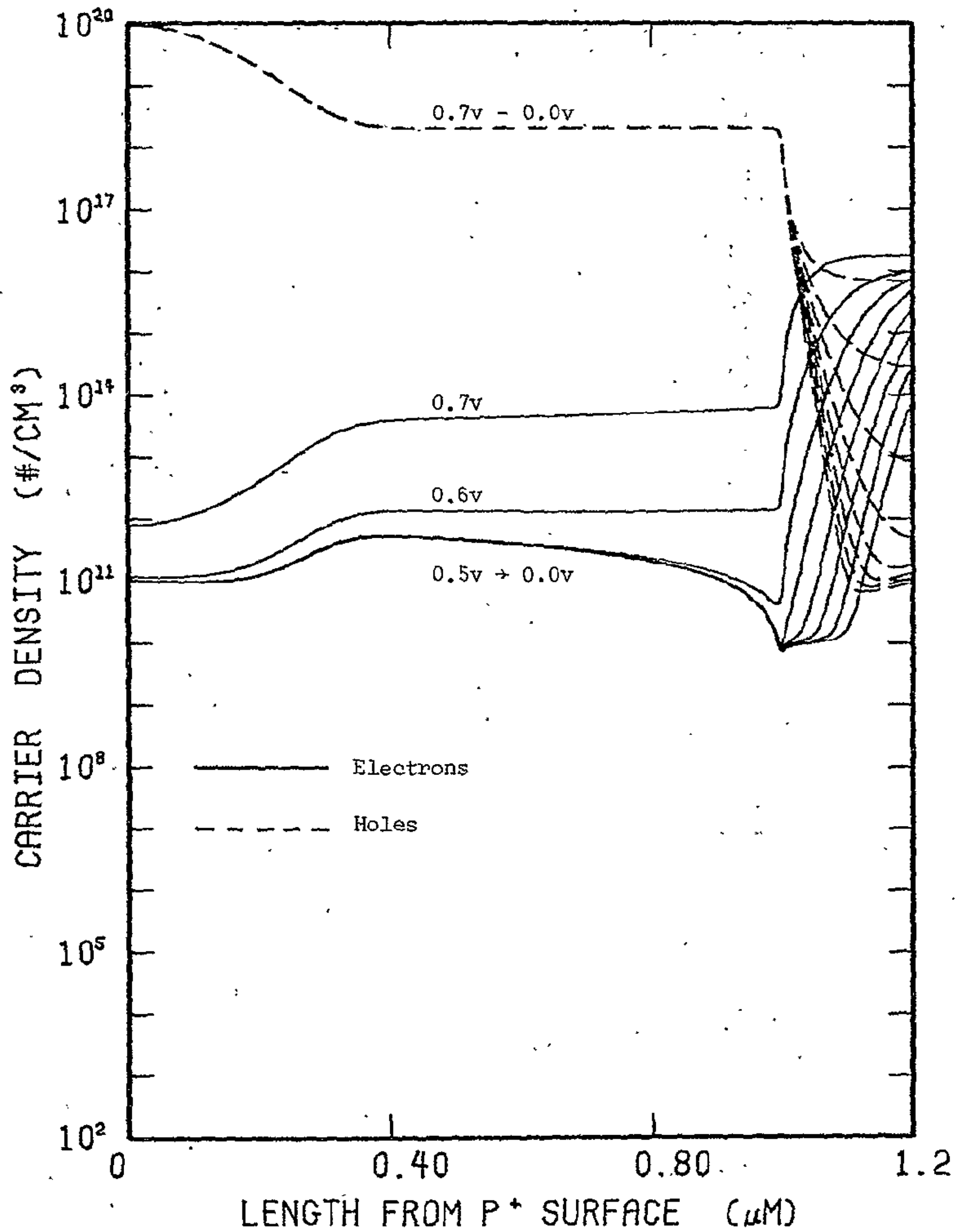

Figure 6.8 Carrier distribution in the surface region for the D'Aiello structure under AMO illumination.

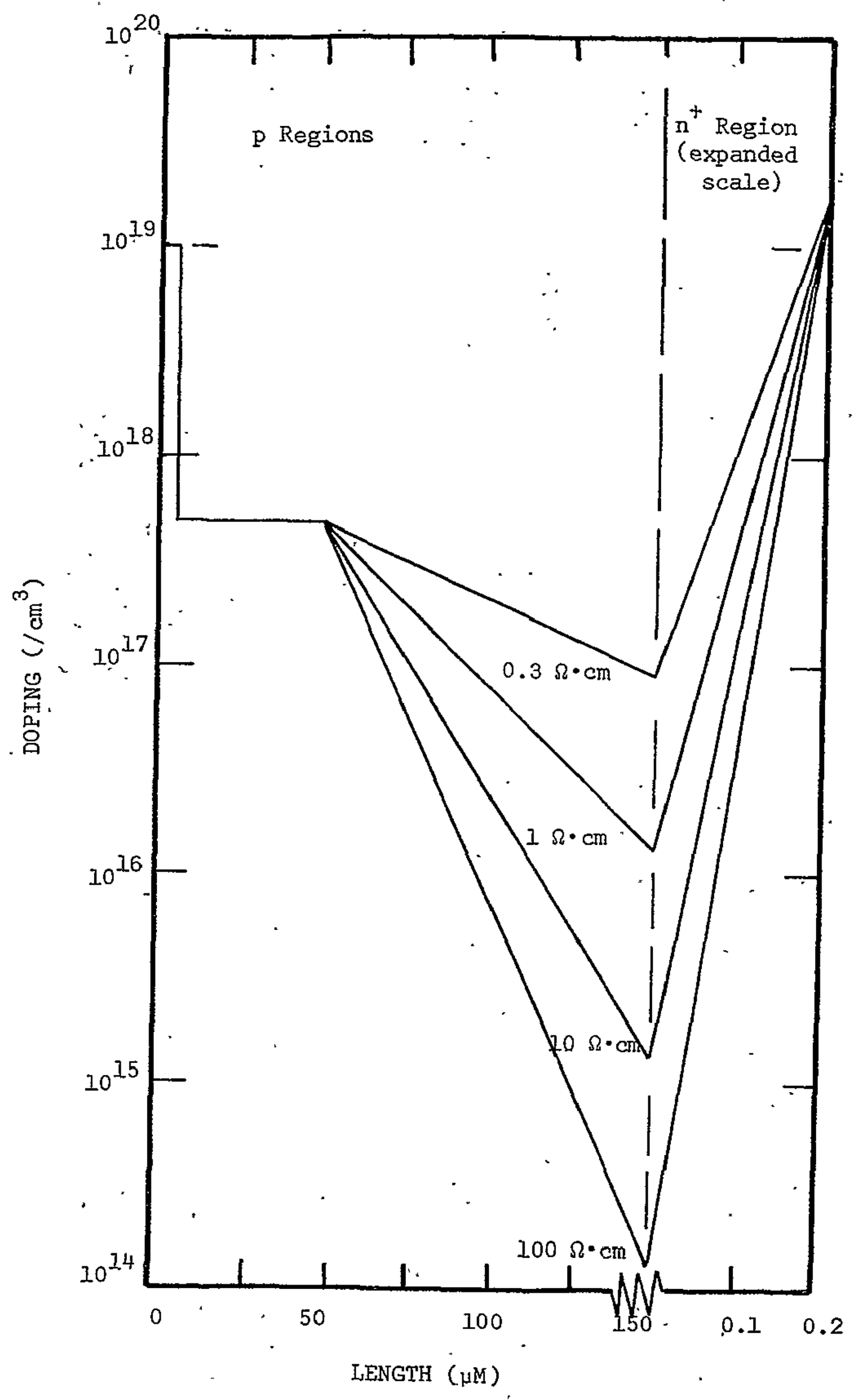

Figure 6.9 Doping profiles for the modified epitaxial structure analyzed in this chapter. Resistivity values near the junction but on the p-side are ∿ 100 Ω·cm, 10 Ω·cm, 1 Ω·cm and 0.3 Ω·cm.

current. However, the back surface p^+ and front surface n^+ regions are narrower than the prior device. In addition, the doping in these regions has been reduced due to lifetime and bandgap reduction considerations. The grading in the base region does not extend throughout the region in order to maintain a reasonable lifetime deep in the device and still set up a large electric field within the center region. The surface region profile is exponential as opposed to Gaussian in order to reduce the extent of severe heavy doping effects and give a constant built-in field. The surface concentration of $2x10^{19}/cm^3$ was selected to minimize heavy doping effects. A 5 per cent film was assumed as an antireflection layer.

The dark characteristics of these devices are shown in Figure 6.10. As seen from these curves the more lightly doped devices tend to approach a common curve at large currents. Due to this the open circuit voltage is not changed significantly for these doping ranges. The surface region lifetime was modeled spatially through an application of the doping dependent data of Iles. With this model, the back injection component of current was about 20 per cent of the total dark current. However, heavier doping at the junction does not reduce the forward current density significantly for the 0.6 V to 0.7 V region.

The illuminated results are collected in Figure 6.11. It can be seen that the efficiency peaks when the resistivity near the p-n junction is about 1 ohm-cm. This peak is due to the removal of high injection operating conditions as evidenced by the rise in the curve factor. A higher doping at the junction further increases the curve factor and the open circuit voltage but at the expense of short circuit current.

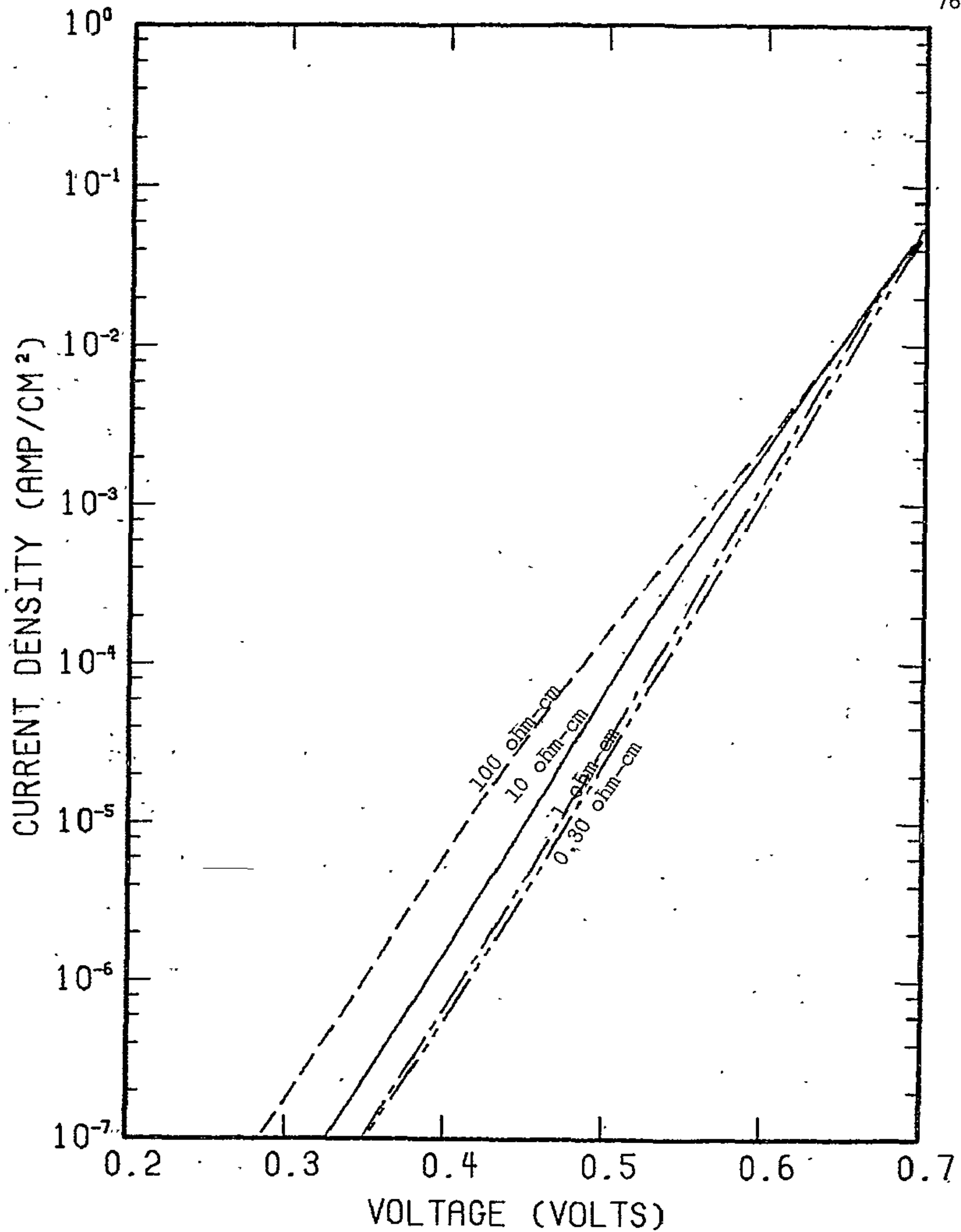

Figure 6.10 Dark J-V characteristics of the modified epitaxial structure described in Figure 6.9. Resistivity values refer to the resistivity near the junction on the p-side.

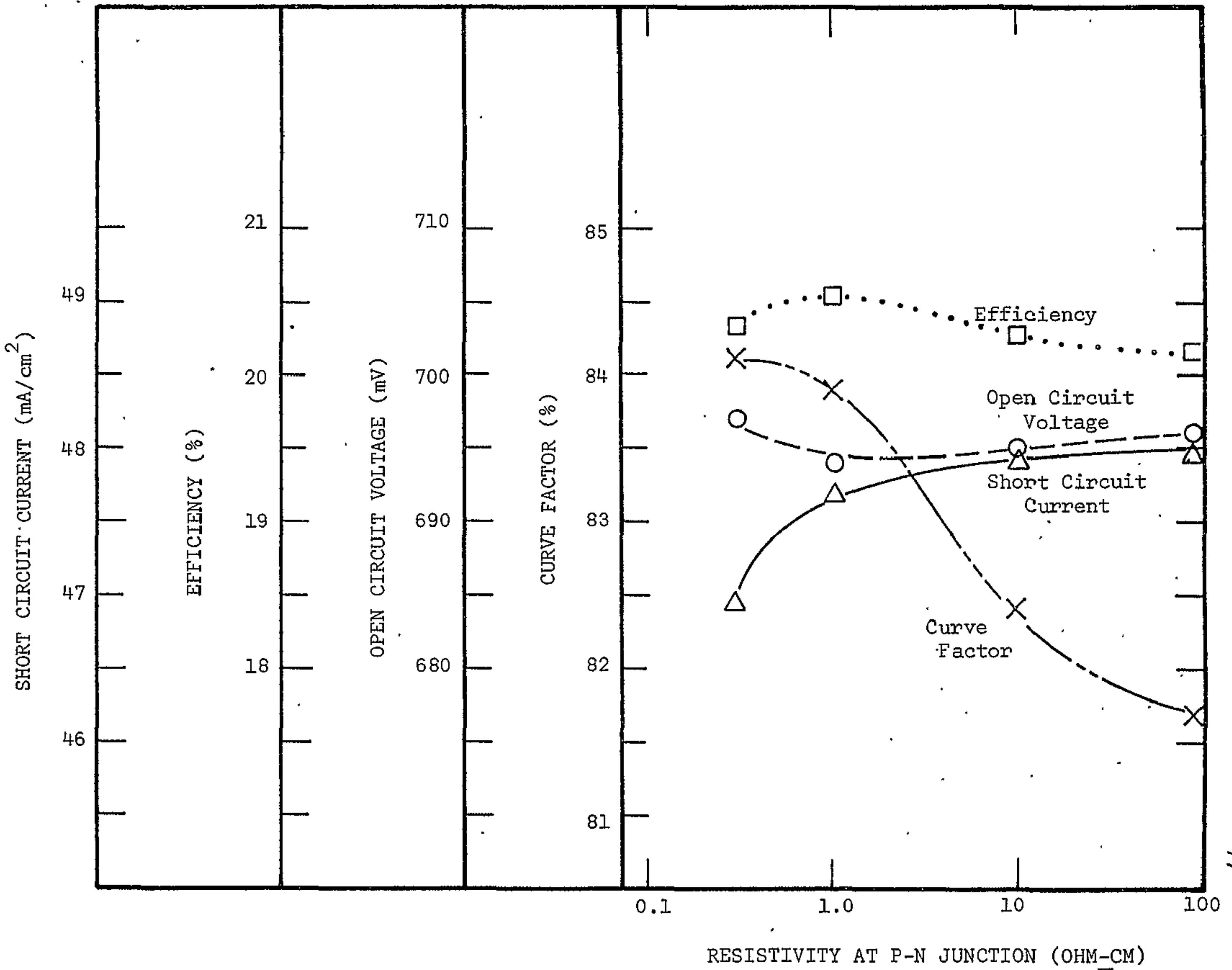

Figure 6.11 Summary of terminal characteristics of the modified epitaxial structure of Figure 6.9.

In comparing this structure with D'Aiello's configuration, the effect of the 800 Å SiO layer must be compensated for since the latter structure utilized the 5 percent layer. In doing this, the D'Aiello structure results in a peak efficiency of about 16.4 percent as compared to the 20 percent efficiency with the latter structure. This difference is due primarily to the loss of collection efficiency in the D'Aiello structure. In spite of the graded base region in the structure, the wide back surface region and front surface region simply allowed too much recombination of the optically generated carriers.

6.2 "Upside Down" Structure

The so called "upside down" structure shown in Figure 6.12 has attracted some interest in the literature due mainly to the removal of shadow effects caused by irradiated surface contact geometries. There is also the ability to reduce series resistance effects by means of thicker contact fingers on the back surface. Such a structure has been analyzed. This 100 μM device includes a 5 μM, n^+ region with an exponential doping profile, a uniform p region, and a narrow 2 μM, exponential p^+ region at the surface to reduce losses to surface recombination. The center region resistivity is 0.3 ohm-cm, whereas the surface and junction region are exponentially graded to $2x10^{19}/cm^3$. Heavy doping is included throughout the device, and a total 5% surface reflection plus total optical reflection at the back surface is also included. The back surface is considered ohmic, while the front surface was modeled with a surface recombination velocity of 100 and 1000 cm/sec. The lifetime for all regions was taken from the data of Iles.

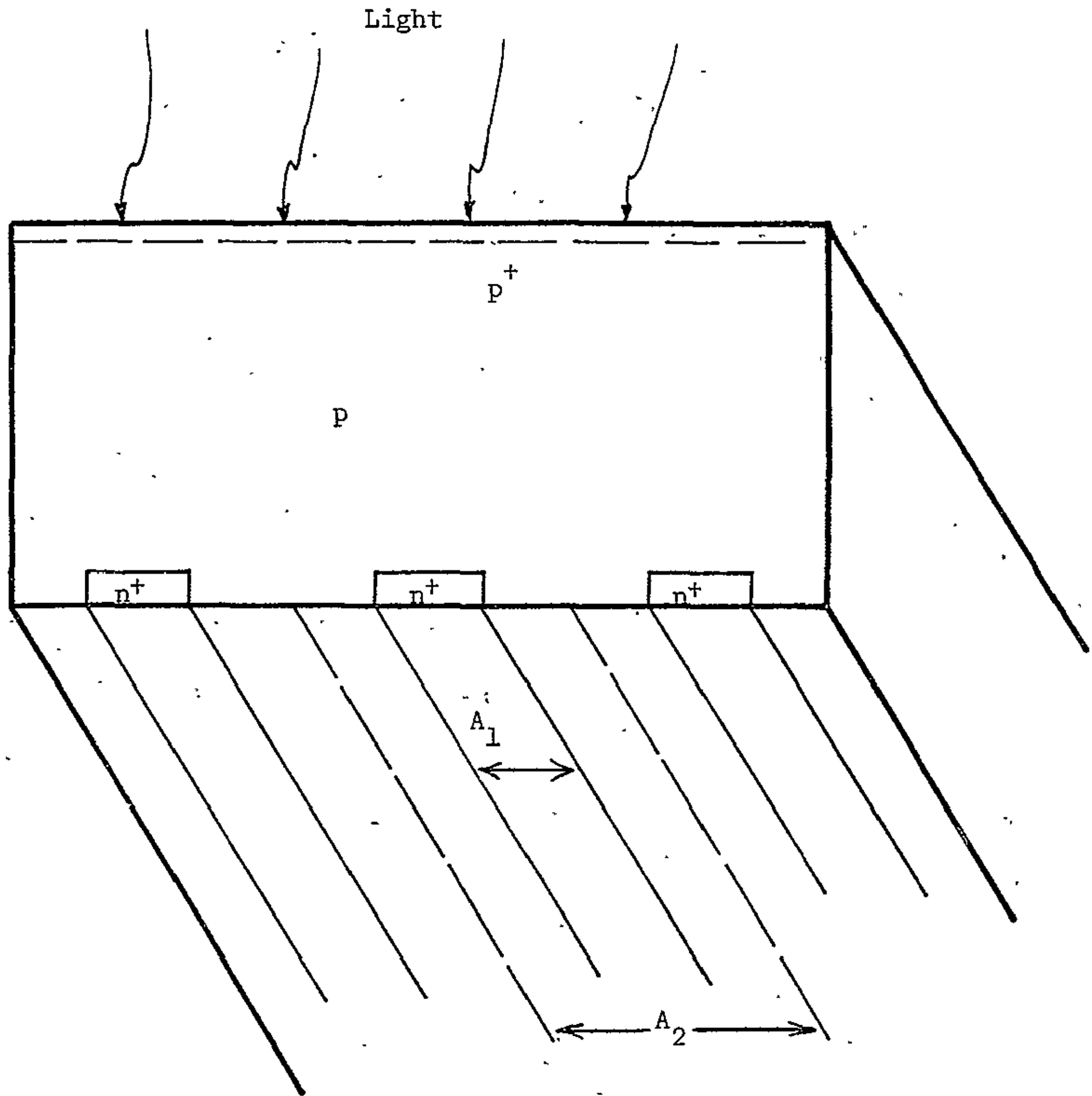

Figure 6.12 General arrangement of the "Upside Down" structure.

The analysis is a one dimensional analysis of a p^+-p-n^+ device of area A_1 (see Figure 6.12). Due to this method of analysis, area corrections must be made to take into account the effect of the additional area A_2. For example, the total electron current injected into the center p region will consist of the depletion region recombination current ($J_n(dep)$) and the bulk region recombination current, $J_n(rec)$. The former is dependent upon the junction area A_1, while the latter is dependent upon the total area, A_2. Both components of the hole current are dependent on the junction area A_1. These components are shown in Figure 6.13. Using these definitions, the total forward current can be written as:

$$I_f = J_n(rec) \cdot A_2 + J_n(dep) \cdot A_1 + J_p \cdot A_1. \tag{6.1}$$

Or, reducing this to a current density based upon the area A_1,

$$J_f = J_n(rec) \frac{A_2}{A_1} + J_n(dep) + J_p. \tag{6.2}$$

Consequently, the bulk electron current must be isolated and multiplied by the area ratio. This is readily done in the complete computer analysis.

Likewise the short circuit current must be broken up into the two components of hole and electron current:

$$I_{sc} = J_n(sc) \cdot A_2 + J_p(sc) \cdot A_1 \tag{6.3}$$

Or,

$$J_{sc} = J_n(sc) \frac{A_2}{A_1} + J_p(sc), \tag{6.4}$$

where J_{sc} is based upon A_1. Since $J_p(sc)$ in that current collected within the narrow n^+ region, it can be neglected as compared to $J_n(sc) \cdot \frac{A_2}{A_1}$. Consequently the total current may be written as

$$J_{TOT} = J_{sc} - J_f, \tag{6.5}$$

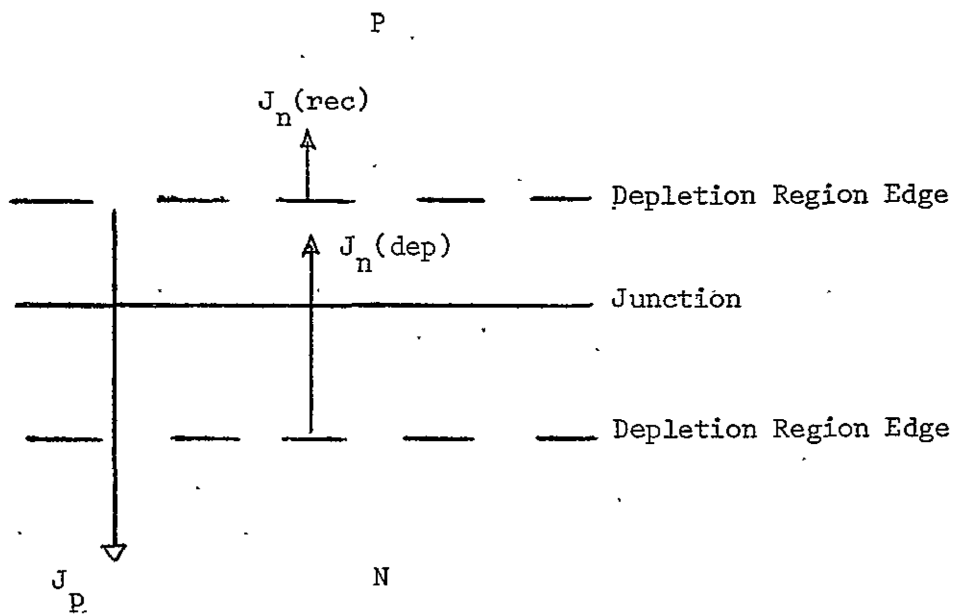

$$I_f = J_n(\text{rec}) \cdot A_2 + J_n(\text{dep}) \cdot A_1 + J_p \cdot A_1$$

or

$$J_f = J_n(\text{rec}) \frac{A_2}{A_1} + J_n(\text{dep}) + J_p$$

Figure 6.13 Area dependence of the current components of the "upside down" cell.

or,

$$J_{TOT} \simeq J_n(sc) \frac{A_2}{A_1} - J_n(rec) \frac{A_2}{A_1} + J_n(dep) + J_p . \quad (6.6)$$

In addition, the spectral irradiance factor must be reduced to the area A_1. This allows the overall efficiency to be written as:

$$\text{Efficiency} = \frac{J_{TOT} \cdot V}{135.3 \text{ mW/cm}^2} \cdot \left(\frac{A_1}{A_2}\right) . \quad (6.7)$$

The results of the analysis is illustrated in Table 6.1. It is seen that the 0.1 ohm-cm base resistivity is too low for the lifetime model and device width utilized. It is also seen that the area ratio is not a strong factor in the overall efficiency. If one combines Equation 6.6 and 6.7, neglecting J_n(dep) and J_p, it can be seen that the dependence upon the area ratio is quite small. As expected, there is little dependence on surface recombination.

6.3 Summary

The various structural modifications studied in this chapter resulted in some devices with conversion efficiencies in the range of 19 to 20 percent. These structures however ranged from rather complex epitaxial type tailored profiles to the relatively simple upside down structure. One conclusion from this study subsequently tends to cast doubt upon the feasibility of resorting to tailored doping profiles for the purpose of increasing collection efficiency. Prior chapters have illustrated efficiencies within the same range with rather conventional, optimized structures. However, the question of lifetime dependence is still a variable which can effect these conclusions. Structures with relatively large center region lifetimes will have good collection efficiencies regardless of a doping profile. Likewise, for poor lifetime material, the collection efficiency will not be substantially increased through tailoring techniques.

Table 6.1 Summary of the terminal characteristics for the "upside down" cell.

	0.1 ohm-cm p region $S=10^2$ cm/sec			0.3 ohm-cm p region $S=10^2$ cm/sec			0.3 ohm-cm p region $S=10^3$ cm/sec		
A_2/A_1	30	10	5	30	10	5	30	10	5
V_{oc} (mV)	697	694	690	704	700	696	702	698	694
Efficiency (%)	15	15	14.9	19.5	19.5	19.4	19.2	19.2	19.1
J_{sc}, based upon A_1 (mA/cm^2)	1044	348	174	1350	450	225	1332	442	222

The exception to this is of course the fields associated with a back surface high low junction. This has been seen to be necessary to obtain reasonable collection efficiencies.

7. SUMMARY

The overall objective of the present work is to continue the identification and characterization of various mechanisms which limit the conversion efficiency of silicon solar cells. In addition, various geometric factors were studied with regard to optimization of the conversion efficiency of silicon solar cells. This includes doping/width modifications on the basic three layered BSF type of cell and more complex modifications which involve tailored doping profiles and four layered structures. This includes both the n^+-p and p^+-n polarity devices. This study has been accomplished by means of a computerized semiconductor device analysis program which obtains a complete numerical solution of the general semiconductor device equations including an excess carrier generation rate due to full spectrum solar irradiance. One overriding factor in the analysis is the lifetime dependence on doping. Virtually all of the work reported here has been carried down to the point where decisions regarding an optimum geometry or doping profile is limited by uncertainty pertaining to lifetime. This includes not only the lifetime of the bulk material but also the nature of the lifetime in heavily diffused regions.

With regard to geometric and doping variations aimed at the optimization of the basic three layered BSF device, the results can be summarized with reference to Figure 7.1. This figure depicts the improvements in efficiency predicted by the various processing optimizations. The peak efficiencies shown do not include shadow or series resistance effects due to contact finger arrangements. These effects can combine to lower the

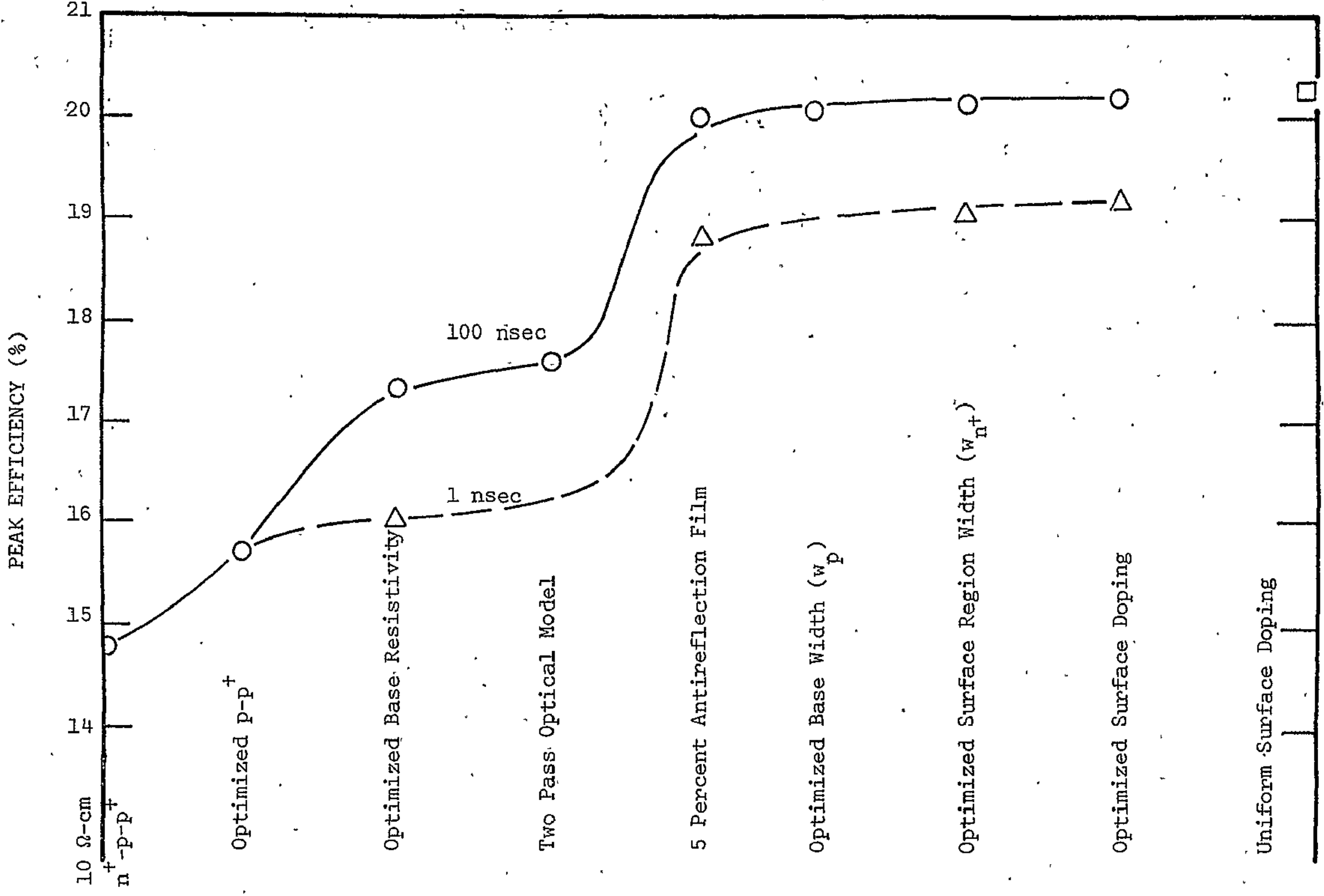

Figure 7.1 Summary of improvements in conversion efficiency afforded by various processing modifications.

calculated efficiencies from 1 to 1.5 percentage points from the values indicated in Figure 7.1. The plot begins on the left with the predicted efficiency of a 10 ohm-cm, 250 μM n^+-p-p^+ solar cell. This initial cell had a n^+ region width of 0.25 μM, and a p^+ width of 0.5 μM with a doping of $10^{18}/cm^3$. For comparison, the 10 ohm-cm n^+-p cell without a high-low junction resulted in efficiencies below 13 percent. All the results shown include heavy doping effects, but have a constant lifetime model in the diffused region.

The first improvement on this basic cell involved the optimization of the p-p^+ high-low junction. This entailed a widening of the p^+ width to 5 μM and an increase of doping to $10^{19}/cm^3$. The next aspect is the selection of a 0.3 ohm-cm base resistivity. At this point, the forward injection component of dark current has been so reduced that the back injection component becomes very significant. Since this component is strongly dependent upon surface region lifetime, the results at this point must be split into high and low lifetime cases. It is evident that a low n^+ region lifetime overcomes almost all of the advantages of optimizing the base resistivity. The next processing improvement is the "two pass" model which includes reflection at the back contact. The improvement gained in the 250 μM cell is slight, but for a narrower cell the improvement is significant as described in the main body of the report. As also seen, the 5% reflecting coating improves the efficiency very significantly.

The next improvement is an optimization of the base region width which shows some improvement in efficiency provided back surface reflection is included. Realize that as one progresses to the right on the chart, process modificationsto the left are included. The optimization of the

n^+ region width did not have significant effects for the high lifetime case but it did aid in the case of a low lifetime surface region. The last two modifications include an optimized surface profile (with respect to retrograde field effects) and a look at a uniform profile in the surface region.

A major result of the foregoing modifications is the conclusion that narrow base width (100 μM) solar cells can be fabricated without a loss in conversion efficiency if optical reflection can be obtained at the back surface. Essentially the same results are obtained with the p^+-n-n^+ polarity device. However, the differences in doping magnitudes which would produce optimum operation in comparison to the n^+-p-p^+ device depend strongly upon lifetime assumptions.

A major aspect of the present work is related to the problems revolving around the lifetime in the surface region. Optimization of the base region resistivity always leads to the situation where the component of dark current which is injected into the surface region becomes dominant. The magnitude of this component is dependent not only upon the magnitude of the lifetime within the surface region but also upon its spatial nature. Also, heavy doping effects in this region tend to interact with a spatial lifetime to produce significant increases in dark current. These increases are exhibited as reductions in open circuit voltage. These results are summarized in Figure 7.2. The devices compared in this figure are optimized narrow base 0.3 ohm-cm solar cells. From this figure, the reduction in open circuit voltage due to heavy doping effects are evident. However, with the model for a constant lifetime in the surface region it can be seen that heavy doping effects are not as severe as in the case where a

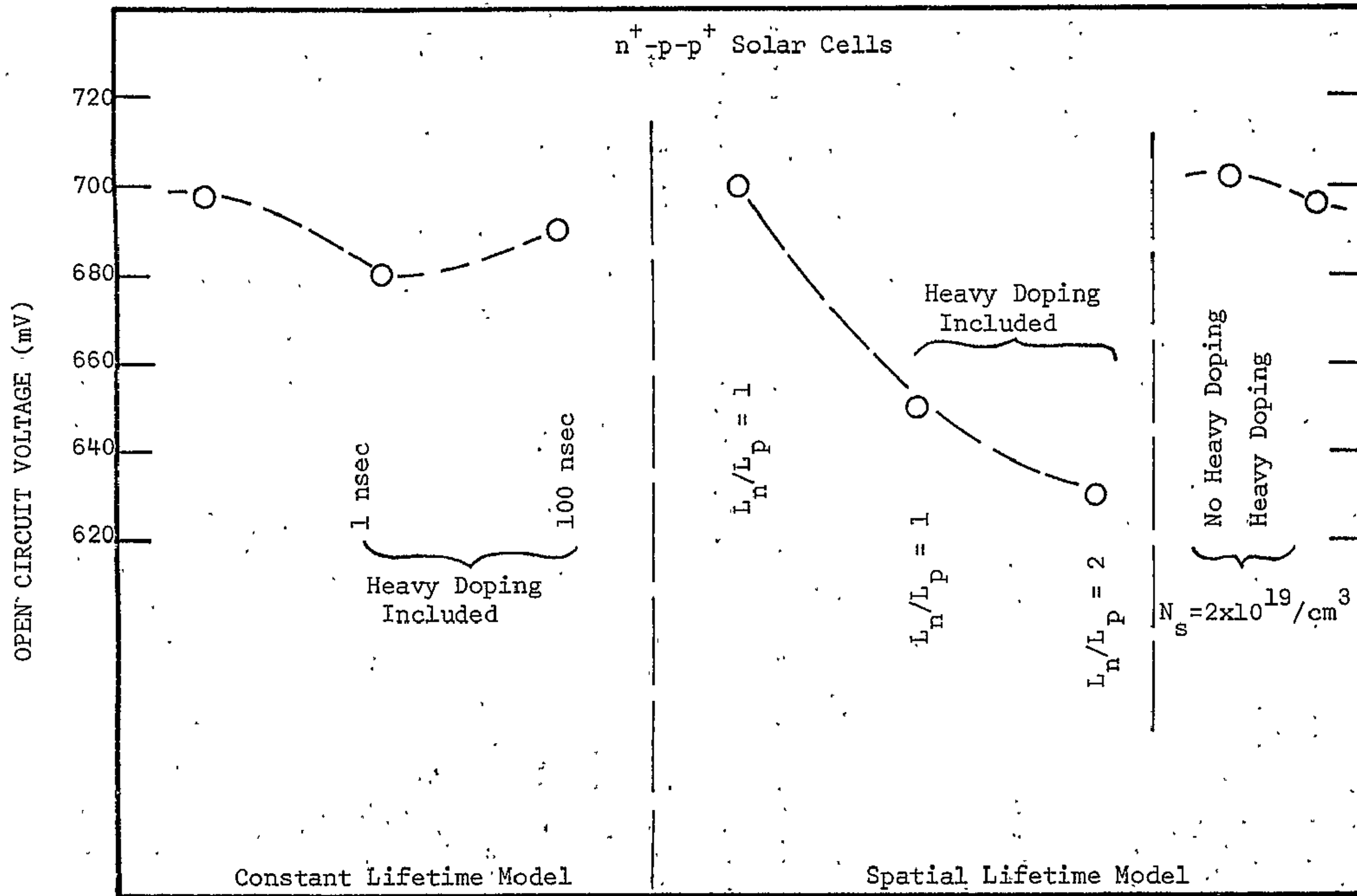

Figure 7.2 Summary of the effects of the lifetime and heavy doping model upon the open-circuit voltage of n^+-p-p^+ solar cells.

spatially dependent lifetime is included. Also included in the figure is the case in which the hole and electron diffusion lengths differ by a factor of two. This difference reduces the lifetime in n-type material. For the n^+-p-p^+ structure the overall magnitude of the spatially dependent lifetime in the surface region is reduced. This causes high dark surface region currents and consequently reduces the open circuit voltage. For the p^+-n-n^+ structure, the unequal diffusion length approximation reduces the base region lifetime, causing mainly an increase in the dark current component injected into the base region, again lowering the open circuit voltage. These comparisons are illustrated in Figure 7.3. Note also that heavy doping effects are less severe in a p-type region.

From these calculations it can be concluded that heavy doping effects combined with a spatially dependent lifetime can form a severe limitation to the open circuit voltage. Spectral response calculation have also indicated that a dead layer can also be formed through the interaction of lowered lifetime and retrograde fields due to band gap reduction at the surface. As shown in Figure 7.2 these effects can be overcome to a large extent in the n^+-p-p^+ device through a selection of a surface concentration which would eliminate the retrograde field.

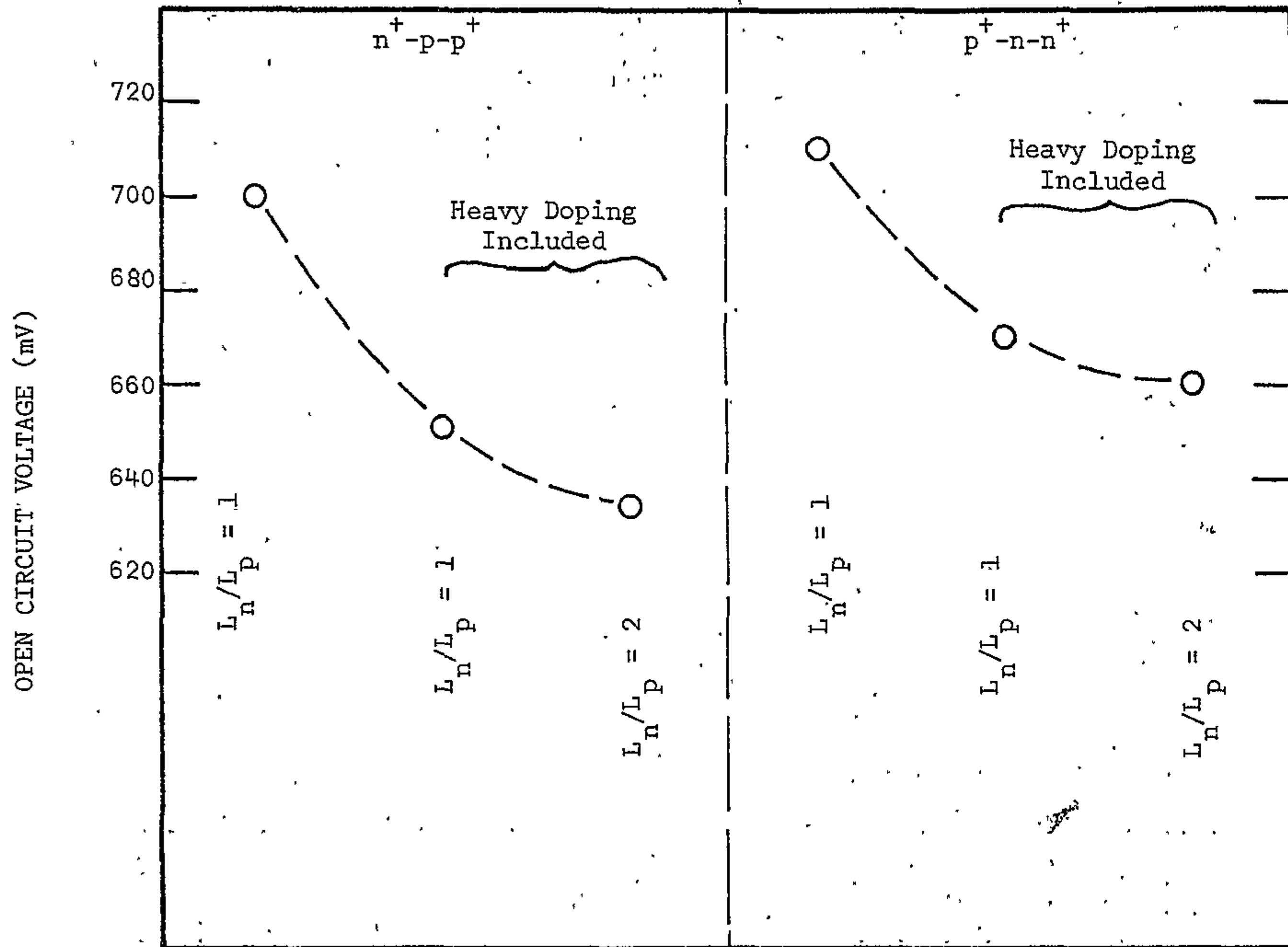

Figure 7.3 Effects of spatial lifetime and heavy doping models upon n^+-p-p^+ and and p^+-n-n^+ solar cells.

8. LIST OF REFERENCES

Brandhorst, H. W. 1975. Current Status of Solar Cell Technology. International Electron Devices Meeting. IEEE Press, New York, New York.

Dunbar, P. M. and J. R. Hauser. 1975. Efficiency of silicon solar cells as a function of base layer resistivity. Eleventh Photovoltaic Specialists Conference, IEEE Press, New York, New York.

Dunbar, P. M. and J. R. Hauser. 1976. A study of efficiency in low resistivity silicon solar cells. Solid State Electronics 19: 95-102.

Fossum, J. G. 1975. Numerical analysis of back surface field silicon solar cells. International Electron Devices Meeting. IEEE Press, New York, New York.

Godlewski, M. P., C. R. Baraona, and H. W. Brandhorst. 1973. Low high junction theory applied to solar cells. Tenth Photovoltaic Specialists Conference. IEEE Press, New York, New York.

Godlewski, M. P., H. W. Brandhorst and C. R. Baraona. Effects of high doping levels on silicon solar cell performance. Eleventh Photovoltaic Specialists Conference. IEEE Press, New York, New York.

Hauser, J. R. 1969. Minority carrier transport in heavily diffused semiconductor devices. Final report on NSF Grant GK-1615.

Heitmann, W. 1971. Properties of evaporated SiO_2, SiO_xN_y, and TiO_2 films. Applied Optics. 10(12): 2685-2689.

Iles, P. A., and S. I. Soclof. 1975. Effect of impurity doping concentration on solar cell output. Eleventh Photovoltaic Specialists Conference. IEEE Press, New York, New York.

Knausenberger, W. H. and R. N. Tauber. 1973. Selected properties of Pyrolytic TA_2O_5 Films. Journal of the Electrochemical Society. 120(7):927-931.

Lindholm, F. A., S. S. Li and C. T. Sah. 1975. Fundamental limitations imposed by high doping on the performance of pn junction silicon solar cells. Eleventh Photovoltaic Specialists Conference. IEEE Press, New York, New York.

Michel, J., A. Mircea, and E. Fabre. 1975. Computer analysis of back surface field silicon solar cells. Journal of Applied Physics. 46 (11): 5043-5046.

Mock, M. S. 1973. Transport equations in heavily doped silicon and the current gain of a bipolar transistor. Solid State Electronics 16: 1251-1259.

Nilsson, N. G., and K. G. Svantesson. 1972. The spectrum and decay of the recombination radiation from strongly excited silicon. Solid State Communications. 11: 155-159.

Revesz, A. G. 1973. Vitreous oxide antireflection films in high efficiency solar cells. Comsat Technical Review. 3(2): 449-452.

Revesz, A. G., J. F. Allison and J. H. Reynolds. 1976. Tantalum oxide and Niobium oxide antireflection films in silicon solar cells. Comsat Technical Review. 6(1).

Slotboom, J. W. and H. C. de Graaff. 1975. Experimental determination of the bandgap in the base region of bipolar transistors. 1975 International Electron Devices Meeting, IEEE Press, New York, New York.

Traina, T. S. and V. A. Mukin. 1966. Electrical and optical properties of titanium dioxide films. Soviet Physics Journal. 6: 40-43.

Van Overstraeten, R. J., H. J. DeMan, and R. P. Mertens. 1973. Transport equations in heavily doped silicon. IEEE Transactions on Electron Devices. ED-20 (3): 290-298.

Wang, E. Y., F. T. Yu, V. L. Simms, H. W. Brandhorst, and J. D. Broder. 1973. Optimum design of antireflection coating for silicon solar cells. Tenth Photovoltaic Specialists Conference. IEEE Press, New York, New York.

Young, L. 1958. The determination of the thickness, dielectric constant, and other properties of anodic oxide films on Tantalum from the interference colours. Proceeding of the Royal Society of London. A 244 (41): 41-53.